IEEE Access
Multidisciplinary | Rapid Review | Open Access Journal

Received November 14, 2019, accepted December 13, 2019, date of publication December 26, 2019,
date of current version January 14, 2020.

Digital Object Identifier 10.1109/ACCESS.2019.2962636

Tactile Sensors for Minimally Invasive Surgery: A Review of the State-of-the-Art, Applications, and Perspectives

NAGHMEH BANDARI[1,2], JAVAD DARGAHI[1], (Member, IEEE), AND MUTHUKUMARAN PACKIRISAMY[2]

[1]Robotic Surgery Laboratory, Mechanical Engineering Department, Concordia University, Montreal, QC H3G 1M8, Canada
[2]Optical-Bio Microsystems Laboratory, Mechanical Engineering Department, Concordia University, Montreal, QC, Canada

Corresponding author: Muthukumaran Packirisamy (pmuthu@alcor.concordia.ca)

The work of Naghmeh Bandari was supported by an FRQNT Ph.D. scholarship, FRQNT CCTT award, and Concordia Public Scholar award. The work of Javad Dargahi was supported by an NSERC Discovery grant and an NSERC CREATE grant for the Innovation-at-the-Cutting-Edge(ICE). The work of Muthukumaran Packirisamy was supported by an NSERC Discovery grant and a Concordia Research Chair grant.

ABSTRACT Minimally invasive surgery has been one of the most significant evolutions in medicine. In this approach, the surgeon inserts specially-designed instruments through a small incision on the patient's skin into the body cavities, abdomen, veins or, arteries and performs the surgery on organs. As a major limitation, surgeons lose their natural tactile perception due to indirect touch on the organs. Since the loss of tactile perception compromises the ability of surgeons in tissue distinction and maneuvers, researchers have proposed different tactile sensors. This review is to provide researchers with a literature map for the state-of-the-art of tactile sensors in minimally invasive surgery, e.g. in robotic, laparoscopic, palpation, biopsy, heart ablation, and valvuloplasty. In this regard, the pertinent literature from the year 2000 on sensing principles, design requirements, and specifications were reviewed in this study. The survey showed that size, range, resolution, variation, electrical passivity, and magnetic-resonance-compatibility were the most critical specification to study for tactile sensors. Based on the results, some of the requirements, e.g., magnetic-resonance-compatibility and electrical passivity are of less generality and more application-dependent; however, size, resolution, and range specifications differ for various applications and are of utmost importance.

INDEX TERMS Electrical sensors, minimally invasive surgery, optical sensors, robotic surgery, tactile sensors.

I. INTRODUCTION

Minimally invasive surgery (MIS) has been the preferred surgical approach over the conventional open surgery due to various advantages. MIS approach allows the surgeon to reach the internal anatomy through small skin incision using specifically-designed low-profile surgical instruments or flexible catheters [1]. As a result, MIS reduces the anesthesia time, incision size, intraoperative blood loss, postoperative infection, trauma, and hospitalization time [2]. With the emergence of robots in MIS, the accuracy and dexterity of manipulation of surgical instruments were considerably improved [2]. Furthermore, the surgeon's physical fatigue and ionizing radiation exposure have been decreased via robotic-assisted minimally invasive surgery (RMIS) [3]. Despite the outstanding advantages of manual MIS and robotic MIS (RMIS), several limitations exist for surgeons. For example, due to the indirect access to the anatomy surgeon's hand-eye coordination, the field of view, and the workspace of the tools are compromised. Most importantly, surgeons lose their natural sense of touch, which results in limited or no haptic perception [4]. Haptic feedback includes kinesthetic (force) and cutaneous (tactile) feedback, the absence of which may adversely affect surgical efficiency and efficacy; thus, resulting in sub-optimal medical treatment [5].

The associate editor coordinating the review of this manuscript and approving it for publication was Gursel Alici.

To tackle this problem, researchers have proposed and developed different tactile sensors to integrate with the surgical instruments and provide surgeons with haptic and tactile information. It is well-known that force feedback helps the surgeon to apply an appropriate force to avoid tissue damage, which is commonly observed as a by-product of loss of haptic feedback and unintentional excessive instrument force [5]. As an instance, da Vinci surgical system (Intuitive Surgical Inc., Sunnyvale, CA), the first and one of the most commercially successful surgical robots to date [3], does not provide the force or haptic feedback. It has been reported that the grasping force would be significantly reduced by force feedback in the da Vinci-performed operations [2].

Utilization of a sensor to measure the tactile cues can ultimately increase the efficiency of the surgery by increasing the surgeon's situational awareness [2], especially for high-risk surgeries, e.g., heart and brain [6]. Such a tactile sensor shall meet specific physical and functional requirements. As instances, surgical instruments like graspers and forceps have small jaws. Therefore, the sensor should be miniaturized to fit at the desired location. Also, the sensor shall be able to work under both static and dynamic conditions, specifically for the moving organs like heart [7].

Similarly, the surgeon may need to hold a tissue by applying a static force continuously [8]. This static force must be constant during the holding period. Also, to avoid tissue laceration the force must not exceed a specific range. However, due to the viscoelastic nature of the tissues, tool-tissue interaction force might diminish over time (a.k.a. stress-relaxation phenomenon), leading to tissue slippage [9]. Another example would be when the procedure is performed under magnetic resonance imaging (MRI). Such a surgical procedure requires the sensor being MRI-compatible. Moreover, in some procedures like cardiovascular MIS, the sensor must be electrically-passive to avoid the interference with the electrical activity of the heart [6], [10].

Tactile sensors for the MIS applications have been mainly developed based on the electrical or optical principles. Fig. 1 shows the categories of tactile sensors for MIS based on their sensing principles. Electrical-based tactile sensors are the most proposed sensing modality for MIS [6], [11]. Electrical sensors can be further categorized as piezoelectric, piezoresistive, and capacitive sensors. Although the electrical-based sensors address most of the requirements mentioned above, are neither MRI-compatible nor electrically-passive. Besides, the piezoelectric-based sensor can not measure the static force. High hysteresis and lack of repeatability are other disadvantages of this category of sensors. On the other hand, optical fiber-based sensors are biocompatible, lightweight, and corrosion resistance. Moreover, optical sensors are electrically passive and work appropriately in MRI environments [12]. This has led to the recent wide adoption of the optical-based sensor for MIS and RMIS [6].

Optical sensors mainly work based on three principles: light intensity modulation (LIM), phase modulation (PM) and, wavelength modulation (WM) [6], [10]. In comparison, the LIM-based sensor provides unique advantages by being inexpensive, thermally insensitive, simple design and easily implementable, while PM-and WM-based types need a relatively expensive measurement system to calculate physical parameters like force and displacement. The downside of LIM-based sensors is that the miniaturization is still a critical issue which limits their scalability. This limitation largely affects the resolution and range of measurement [13], [14].

The design requirements (a.k.a. constraints) for the tactile sensors in MIS applications can be related to the physical and functional properties of the sensors. Physical requirements attribute mainly to the shape and size of the sensors, while the functional constraints relate to the compatibility, interaction, and performance of the sensor at the bio-environment. As an example of physical constraints, an MIS tactile sensor should be small in size and cylindrical in shape to be integrable at the body or tip of a catheter. As a functional requirement, the sensor should be capable of measuring the contact force in a range of 0-5N with a resolution of 0.01N [15]. Furthermore, the sensor should be fairly sensitive, linear, and show a low level of hysteresis.

This review aims to provide an overview of the state-of-the-art of the proposed tactile sensors integrated with the MIS and RMIS surgical instruments. Previous reviews in the literature have mainly focused on either optical or electrical sensors, e.g., [16]. Also, the reviews which covered both principles were not specifically focused on the MIS/RMIS applications, e.g., [17]. To this end, in this review, various types of tactile sensors, the sensing principles, surgical applications, advantages, and limitations were discussed. Also, the theoretical background of the sensing principles and design requirements of the sensors were critically described and compared. Different physical, engineering, and biologic requirements of the tactile sensors, i.e., size, range, resolution, variation, electrical passivity, and MRI-compatibility, were highlighted. In the end, the concluding remarks summarized the current technological obstacles and perspectives for future research and development.

II. METHODOLOGY

Researchers have investigated the physical and functional requirements of tactile sensors for surgical applications from various points of view, e.g., geometrical, mechanical, electrical, and medical specifications. Therefore, the available literature is broad and multi-disciplinary. This review is based on surveying the literature on *Google Scholar, Scopus, Engineering Village, and PubMed*. The period was limited to articles published from the year 2000 to 2019. Keywords used in the searches were logical (*'.AND.'-'.OR.'*) combinations of *'tactile sensor', 'force sensor', 'pressure sensor', 'optical sensor', 'fiber optic sensor', 'MIS sensor','RMIS sensor'*. The duplicate findings were discarded and the remaining papers were reviewed according to their sensing principles with application in MIS/RMIS procedures, e.g., robotic surgery, laparoscopy, palpation probing, biopsy needling, heart

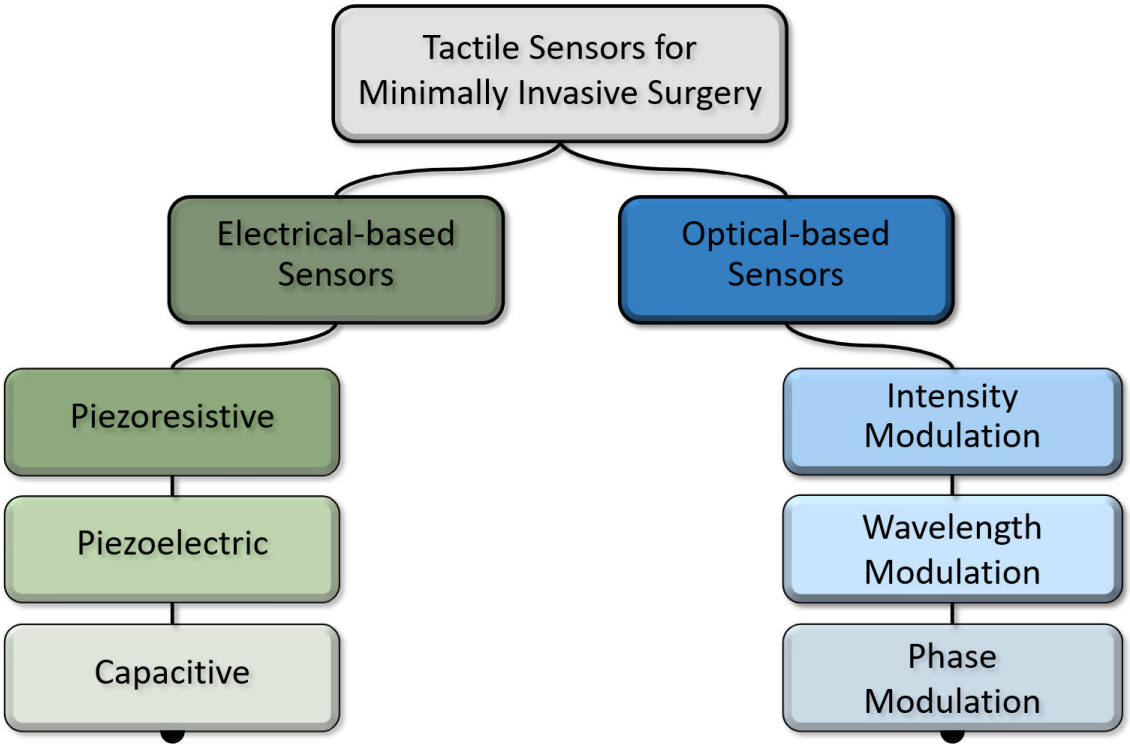

FIGURE 1. Categories of various tactile sensors proposed in the literature for minimally invasive surgery.

ablation, valvuloplasty. The summary of the literature review is provided in Section III.

III. TACTILE SENSORS IN MINIMALLY INVASIVE SURGERY

A. ELECTRICAL-BASED TACTILE SENSORS IN MIS

In the last decade, many tactile sensors have been developed and investigated for MIS/RMIS applications. Although they were mostly research prototypes, a few were commercialized. The application of the sensor is a major factor that imposes physical and functional requirements. Therefore, in choosing a sensing principle, the application factor must be carefully taken into account. Researchers must first define the use-case of the sensor before adopting a sensing principle and developing a sensor upon that.

The most adopted sensing principles for MIS and RMIS tactile sensors are electrical-based sensors [6], [11]. These tactile sensors are further categorized into piezoresistive, piezoelectric, and capacitive sensors. In the following, the electrical-based tactile sensors are summarized. In the end, a summary of verified and validated electrical-based MIS and RMIS sensors are tabulated.

1) PIEZORESISTIVE TACTILE SENSORS

The piezoresistive sensing principle is based on the change in the resistivity of the material cause by a mechanical strain in response to a physical stress, e.g., compressive, shear, thermal stress. The change in the resistance of a (semi-)conductor is a function of its physical dimensions and the material resistivity. The change in the dimensions is exploited mainly in the metallic conductors. For example, strain-gauges have been developed based on the geometrical deformation of strain-sensor-embedded structures. For semiconductors, however, the change in (specific) resistivity is employed [19].

Strain gauges are a popular type of piezoresistive sensors, which are normally thin, long, and zig-zag-patterned conductors. When a conductive material is deformed, its dimension vary in the x, y, and z directions due to its Poisson's ratio. The spatial strains caused by the deformation regulates the variation of the resistance [19], [20] according to Eq. 1.

$$\frac{\Delta R}{R} = (1 + 2\nu)\frac{\Delta L}{L} + \frac{\Delta \rho}{\rho}, \tag{1}$$

where, R, ν, and ρ are the resistance of the piezoresistor, Poisson's ratio, and resistivity, respectively. While $^{\Delta\rho}/_{\rho}$ is negligible in metals and strain gauges, it is noticeable in semiconductors. The change in the resistance can be expressed in terms of the applied pressure, force, temperature or deformation. The applied stress can be further written in terms of the observed strain using a constitutive equation, e.g., linear Hooke's law for springs.

In an early study, Tanimoto *et al.* [21] proposed a micro piezoresistive force sensor for intravascular neurosurgery to measure the interaction force between the catheter with 1.65 mm of diameter and blood vessels. For the first time

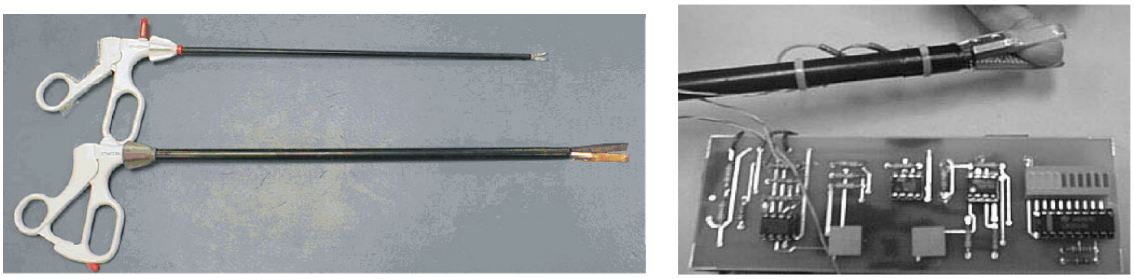

(a) (b)

FIGURE 2. **(a) Two sensorized graspers with microstrain gauges placed at the jaws, (b) electronic feedback system with LED to display the sensor output [18].**

in the world, they evaluated their tactile sensor in a canine animal model. The sensor was comprised of a set of piezoresistive strain gauge on a silicon diaphragm. The silicon diaphragm would deflect due to the applied pressure, and the resistance of the strain gauges would change. The validation was performed for the range of force caused by the blood pressure in healthy circulation, i.e., 60-130 mmHg. Their sensor was capable measuring at a rate of over 2 kHz and successfully captured the fluctuation of blood pressure.

Similarly, Dargahi and Najarian [18] mounted two microstrain-gauge sensors at the back-face of a custom-designed endoscopic grasper. Two different types of the proposed grasper and their associated electronic feedback system is shown in Fig. 2(a). The magnitude of the applied force on the grasper was displayed on a light-emitting diode (LED) display (Fig. 2(b)). Their force senor was working linearly in the range of 0.5 to 10 N with 0.5 N precision. The sensor had high sensitivity and a wide range of measurement suited for the endoscopic surgery. Since endoscopic grasper was to work safely in the liquid-present human body, they encapsulated the sensor with a silicon rubber wrap that sealed the tactile sensor.

King *et al.* [22], [23] integrated a FlexiForce™ piezoresistive force sensor on a surgical tool of the da Vinci system and transmitted the grasping force to the surgeons. Their study revealed that the force feedback could enhance the safety in robotic surgery by reducing the grasping forces during the procedures significantly.

In another effort, Hu *et al.* [24], developed a tactile sensor inspired by the biological hair cells. The hair cells consist of a cilium and a neuron. When an external force or local fluid flow deforms the cilium, the mechanical deformation is conveyed trough the neuron attached to the bottom of the cilium and generates the action. This bioinspired tactile sensor was proposed for robotic end-effector. It was composed of a central silicon post and a bottom polyamide diaphragm with four integrated piezoresistors. Fig. 3(a) illustrates the 3D design, and the view of the bottom surface included the resistors. Bending the silicon post would deform the diaphragm on which piezoresistors were located. As a result, three components of the mechanical forces were captured by four piezoresistors. Having the high aspect-ratio silicon post surrounded by a cylindrical cavity increased the sensitivity of the sensor as well as the measurement range.

To have a structure and size suited for the MIS instrument, a deep reactive-ion etching process was used for the fabrication of their sensor. The micro-needle pushing experiment was done in three directions of X, Y, and Z, while the differential voltages of resistors were recorded for calibration. The experimental results showed the shear and normal force sensitivity of 10.8 $^{V}/_{N}$ and 3.5 $^{V}/_{N}$, respectively. This bio-inspired tactile sensor was a promising device for MIS applications due to its high sensitivity, durability, and simplicity. However, due to the limited lateral displacement of the silicon post, the sensor output would saturate in a shear force greater than 0.05 N. The schematic of their tactile sensor on a printed circuit board mounted on a robotic end-effector and the fabricated sensor with its wire-bonding are shown in Fig. 3(b).

In another study, Zarenia *et al.* [25] sensorized a bipolar forceps to measure tool-tissue interaction force during the neurosurgical procedure. They installed strain gauges sensors to a commercially available bipolar forceps. When the surgeon opens and closes the prongs of the forceps, forces would be applied perpendicular to the longitudinal axis of the prongs. These forces would cause deformation in strain gauges and subsequently change their electrical resistance. They proposed two configurations for the strain gauges. In the first design, for axial measurement, a set of strain gauges were installed on the lateral side of the forceps along the X-axis, as shown in Fig. 4(a). Since in reality, in addition to the axial strain, a lateral strain is occurred by the axial shortening in forceps prongs, a planar configuration with two sets of strain gauges in both X- and Y- axes were developed. Fig. 4(b) depicts the planar configuration. To increase the sensitivity, Zarenia *et al.* used finite-element analysis to optimize the location of the strain gauges on the forceps.

They tested the axial and planar bipolar forceps in five different neurosurgical tasks on two cadaveric brains. In all tasks, the axial forces were less than the planar force. Moreover, their sensorized forceps showed the efficiency of measuring the real-time intraoperative tool-tissue interaction force. Such information would be invaluable for training and evaluating the performance of inexperienced surgeons with sensor-equipped surgical robots and virtual reality simulators.

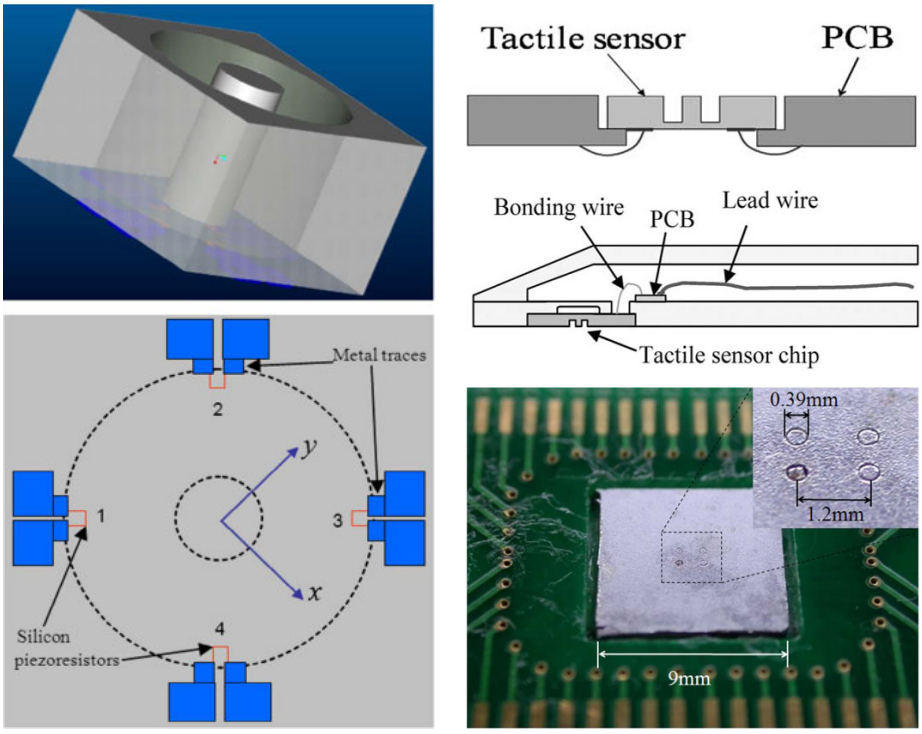

FIGURE 3. Bioinspired piezoresistive tactile sensor by Hu *et al.* [24]: (a) 3D design and the bottom-view of the embedded resistors, (b) microscopic view of the assembled tactile sensor and its associated circuitry.

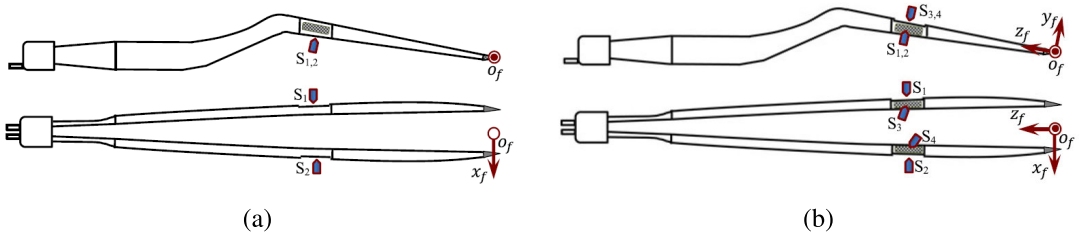

FIGURE 4. Placement of strain gauges on a bipolar forceps: (a) axial sensors, (b) planar sensors [25].

Although piezoresistive tactile sensors exhibit high dynamic range of measurement, high spatial resolution, simple manufacturing process, and durability, their major limitation is hysteresis [17]. Unless compensated, hysteresis decreases the reliability of the system by reducing the sensitivity and repeatability of the tactile sensors [6], [17]. As an option, embedding the piezoresistors in a flexible self-recoverable structure is an option [26]. However, a secondary hysteresis might occur due to the viscoelastic properties of such a structure. Another possibility would be to compensate for the hysteresis through proper nonlinear calibration [13], [27]. A summary of the state-of-the-art piezoresistive tactile sensors postulated for MIS are mentioned in Table 1.

2) PIEZOELECTRIC TACTILE SENSORS

Since 1880, the discovery of the piezoelectric effect led to the most significant revolution in developing transducers and sensors. Also, with the discovery of the piezoelectricity in Polyvinylidene Fluoride (PVDF), it has emerged in the electrical-base sensors in the 60s. Piezoelectricity is the phenomenon of accumulation of electric charge on the surface of a solid due to physical stress. Such accumulation of charge on one surface of a solid produces electrical potential difference across the solid. Consequently, the deformed solid acts as a capacitor. However, since the electric charges tend to migrate from high potential to low potential, and in the absence of a physical barrier, e.g., dielectric, the charges move toward the low potential locations. This makes the piezoelectric phenomenon temporary under constant mechanical stress (static loading). Equation (2) shows the simple mathematical relationships between the electromechanical effects used in the design of piezoelectric sensors [29].

$$V = f\sigma, \tag{2}$$

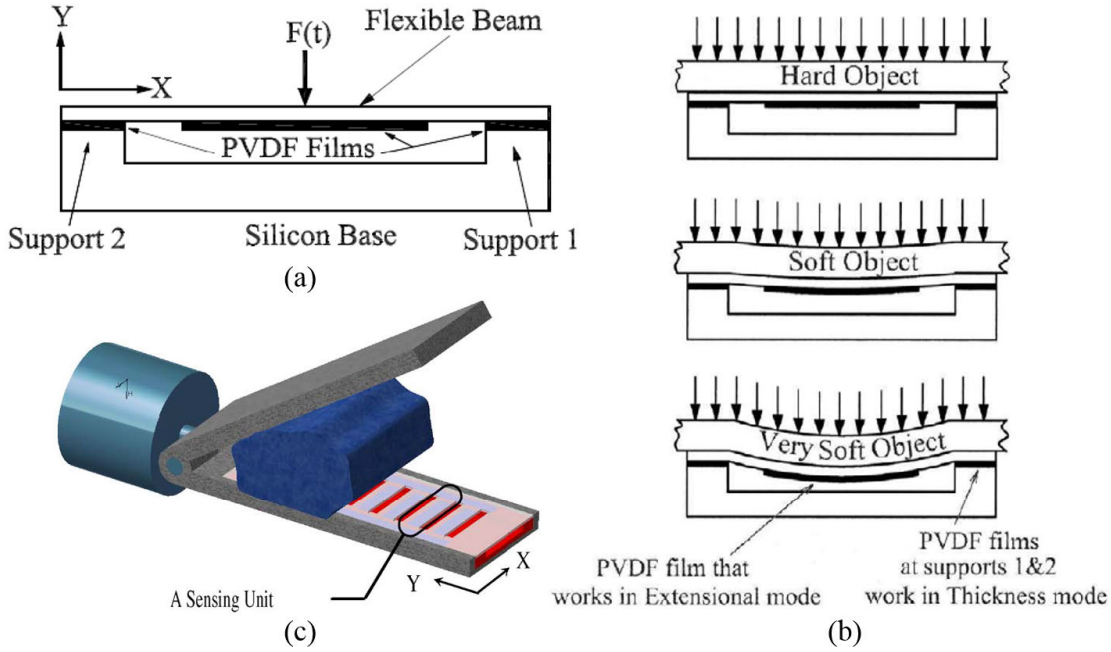

FIGURE 5. (a) cross-section of the sensor structure, (b) a single sensing unit under a typical grasping force, (c) schematic of the equipped grasper with an array of sensing units [28].

where V is the generated electric field in volts per meter and σ, is the induced stress by physical loading. The coefficient f is a constant. The produced mechanical strain is defined by (3):

$$\varepsilon = Vd, \tag{3}$$

d is the piezoelectric coefficient and has the following relationship with f and E Young's modulus of the piezoelectric material.

$$\frac{1}{fd} = E. \tag{4}$$

Equations (3) and (4), are the fundamental expressions to correlate the electrical voltage and physical loading. Similar to the piezoresistive theoretical framework, proper constitutive assumptions can be employed to relate the physical stress to the piezoelectric voltage.

In the last decade, many tactile sensors have been proposed based on the piezoelectric principle. For example, Elkund *et al.* [30] developed a piezoelectric tactile sensor for measuring the tissue stiffness at the tip of a surgical catheter. Their sensor was tested in both silicon and a human prostate model. It was intended to be used for diagnosing prostate cancer. In continuation, Sokhanvar *et al.* [28] proposed piezoelectric-based sensors for application in minimally invasive endoscopic instruments. They utilized the microelectromechanical system (MEMS) technology to fabricate a miniaturized tactile sensor for MIS graspers. To have a sensitive and linear system, they used PVDF film as the transducer to measure the force, force position, and softness of the grasped object. Estimating the relative softness of the object necessitated at least two independent sensors to quantify the applied force on the object and its total deflection. Fig. 5(a) illustrates the cross-section of the sensor structure proposed in [28]. Also, Fig. 5(b) and (c) show a single sensing unit under applied force during a grasping task, and a schematic of the sensor on the grasper, respectively. When the object was grasped, the middle PVDF film would deform and change the sensor's voltage. The voltage was calibrated versus the softness of the object.

Also, the PVDF on support–1 would show the grasping force when the tissue was grasped, while support–2 was used to determine the position of the point load. To validate the sensor performance, firstly, they selected four samples of the materials with known durometers and calculated their compressive Young's modulus, which was in the range of 50 to 280 kPa and hard material with 6 MPa. In fact, each material was a representative of human tissue. Due to the favorable results of their sensor in material distinction and contact point detection, they postulated to use the sensor in an array configuration. However, because of the intrinsic decay of voltage in the piezoelectric sensing element, their sensor was not able to meet the use-case requirements for static loading conditions, e.g., in the constant grasping of tissues. In a similar study, Chuang *et al.* [31] fabricated a miniature piezoelectric tactile sensor to detect submucosal tumors in endoscopic procedures. The sensor was made of a PVDF sensing film and two components consisted of a hard copper ball and polydimethylsiloxane (PDMS) soft outer packaging, as shown in Fig. 6(a). Since these two components had different stiffness, they would sense different deformations under an external force. Therefore, when the

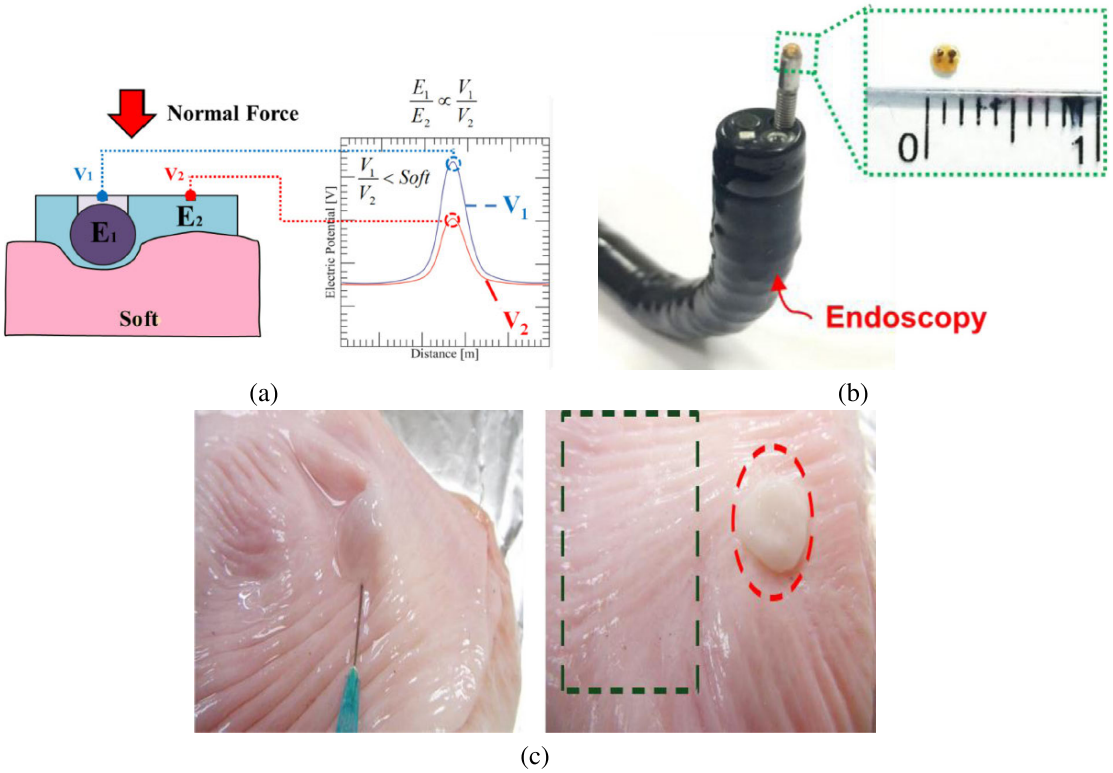

FIGURE 6. (a) schematic of the tactile sensor in interaction with soft tissue, the graph shows the relative output voltage of the sensing elements, (b) endoscope equipped with the tactile sensor, (c) submucosa of a swine stomach with an artificial tumor lump [31].

sensor touched an object, the piezoelectric film under the two components would generate different voltages. The ratio of these two voltage outputs was used to calibrated versus the elasticity of the tested objects. This sensor could be integrated on the endoscope to distinct the hidden tumor from healthy tissues. Their results suggested the feasibility of a sensorized endoscope be used as a diagnostic instrument for faster and more precise treatment. The equipped endoscope with this tactile sensor is illustrated in Fig. 6(b). They proposed an analytical model based on the tandem spring model and change in voltage output of piezoelectric components.

To validate the sensor performance, five different elastomers with known moduli of elasticity were injected into the normal tissue of the pig stomach submucosa. Fig. 6(c) depicts the submucosa of the pig stomach included an artificial tumor. The sensor was able to estimate the elastic moduli of the samples between 1.01 and 3.51 MPa. Their results verified their postulation and were in fair agreement with the theoretical predictions.

In a recent study, Sharma *et al.* [32] introduced a biopsy needle equipped with a piezoelectric sensor. Their system, named as the Smart Touch Fine Needle (STFN) was capable of detecting the variation in tissue stiffness. It was utilized to characterize the thyroid tumor based on its mechanical properties. Studies have shown that malignant thyroid nodule is stiffer than the healthy nodules [33]. Therefore, real-time mechanical characterization of the thyroid nodules would help in the early detection of malignancies.

In [32], the sensor was fabricated using additive manufacturing technology to have a precise and low-cost manufacturing process. A piezo-cylinder was used as a force transducer attached to the fine needle. The electric current induced by the mechanical force on the piezoelectric component was recorded in time. The schematic of the needle embedded with piezoelectric transducer and its experimental diagram is depicted in Fig. 7(a). To calibrate their sensorized needle, they tested it on a series of known stiffness biomaterials. Also, they performed *ex-vivo* experiments on a series of extracted porcine kidneys. The force data during the insertion into the samples were recorded to characterize the tissue stiffness, as shown in Fig. 7 (b).

To evaluate the sensor performance, different malignant thyroid samples of patients were tested and compared with the normal thyroid tissue. Results revealed that the stiffness of normal tissue was 0.06 ± 0.02 mN/mm, while the stiffness for the malignant tissue varied from 0.02 ± 0.00 to 0.41 ± 0.03 mN/mm.

Piezoelectric tactile sensors exhibit high sensitivity and accuracy. In addition, PVDF film transducers are fairly linear and respond at high frequency. However, piezoelectric sensors can not detect static loads. This constitutes their major limitation for surgical applications. Furthermore, piezoelectric sensors are thermal-sensitive, which means their

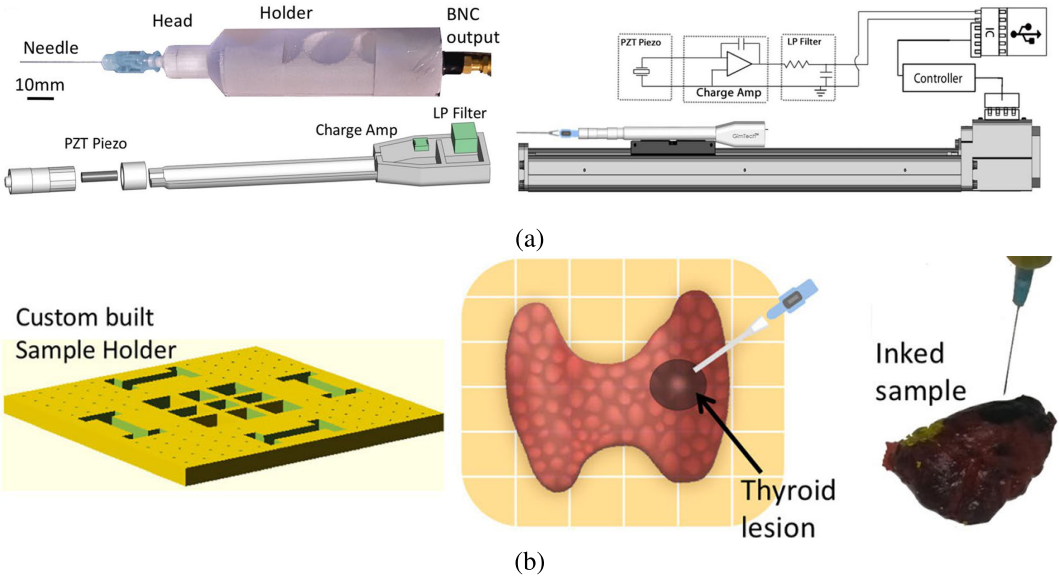

FIGURE 7. (a) schematic of the needle embedded with piezoelectric transducer and its experimental diagram proposed by Sharma *et al.* [32], (b) experimental validation using a thyroid sample.

characteristic equation changes by varying temperatures. In a surgical setup, the sensor is exposed to various temperatures, i.e., from $18 - 20°C$ (operation room temperature) to $37°C$ (core-body temperature). Therefore, thermal sensitivity also hinders its application in MIS and RMIS. A summary of the representative studies on piezoelectric tactile sensors for MIS applications is presented in Table 1.

3) CAPACITIVE TACTILE SENSORS

Capacitive tactile sensors are the next widely used electrical-based sensors in MIS and RMIS. Essentially a capacitor is made of two facing conductive plates with a relatively small gap in between. If an electric potential difference is applied on the two plates, equal and opposite electrical charges are accumulated on both surfaces. An insulator slab (dielectric) might be placed in the gap space to increase the capacitance. The capacitance for two parallel plates, C, is defined by (5), in which Q is the stored charge and V is electrostatic potential. Also, the capacitance can be estimated by employing (6), where A is to perpendicular projected overlap area of the plates, ϵ is the permittivity, and d is the distance between two plates.

$$C = \frac{Q}{V}, \tag{5}$$

$$C = \frac{\epsilon A}{d}. \tag{6}$$

The capacitive sensors work based on relating the change in the voltage of a capacitor to physical variables, e.g., force, pressure, displacement, temperature, or humidity. The way each of the variables changes, i.e., A or d, is usually obtained through the mechanical modeling of the sensor. Afterward, the obtained equation is substituted in (5) and (6) to find the relationship between the physical variable and voltage. For example, normal force and pressure on the plates can change the distance between the plates. Equation (7) shows the relationship between the normal force, F, on the parallel plates and the output voltage of the capacitor.

$$F = \frac{\epsilon A V^2}{2d^2} = \frac{CV^2}{2d}. \tag{7}$$

Researchers have proposed various capacitive tactile sensors for MIS applications. In an early study, Eltaib and Hewit [34] recommended a micromachined capacitive pressure sensor integrated at the end of a tactile probe. The probe was sinusoidally vibrated into the examined tissue. This displacement caused a sinusoidal force on the capacitive sensor. Therefore, the change in capacitance was measured and transformed into the output voltage. The stiffness map of the probed tissue was displayed on a digital graphical contour to inform the surgeon of the difference between soft and hard tissue as a cue for finding abnormalities.

Also, Peng *et al.* [35] proposed a flexible tactile sensor using PDMS as the sensor structural element. PDMS is well-known for having flexibility, ductility, durability, and biocompatibility. Furthermore, PDMS is easy to micro-fabrication for integration with the existing endoscopic instruments. Their sensor was capable of measuring the tissue elasticity and contact force, simultaneously. Fig. 8(a) shows two different sensing elements composed of a flexible membrane within an array of capacitors in the top and bottom of PDMS layers. Upon the contact between the sensor and tissue, the relative deflection of two sensing elements would be measured by the embedded capacitors. Fig. 8(b) depicts a fabricated PDMS tactile sensor in [35]. The sensor calibration was performed by using the sensor on rubber samples with various known hardness. Results verified that the sensor could measure elasticity range from 0.1 to 0.5 MPa with a resolution of 0.1 MPa.

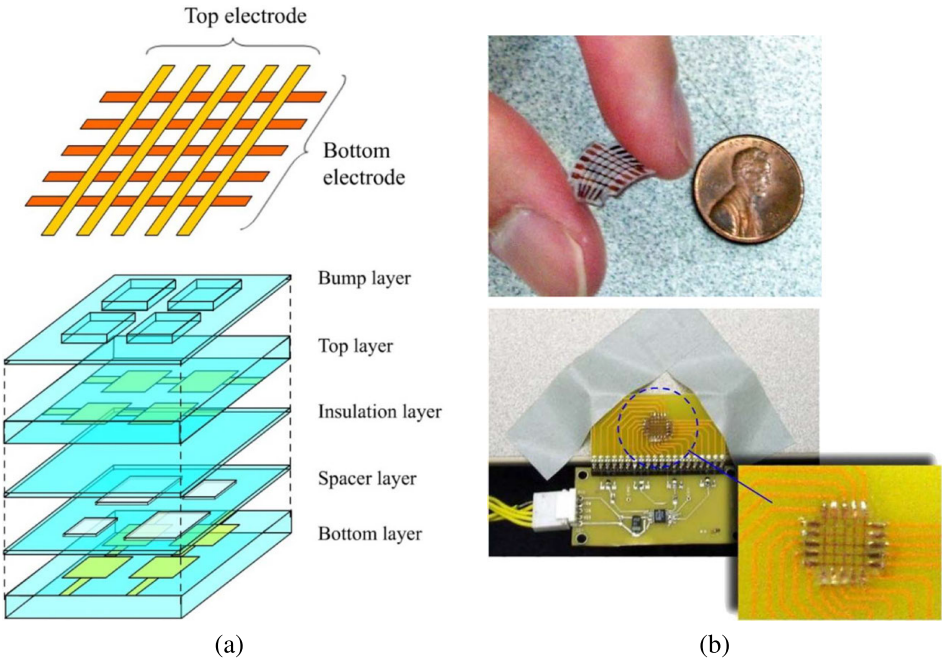

FIGURE 8. (a) schematic of the orientation of electrode and flexible layered structure of the sensor, (b) prototype sensor and its data acquisition system [35].

Paydar *et al.* [36] proposed a miniaturized and low-profile thin-film capacitive force sensor array to integrate with a tactile feedback system for MIS. The sensor was comprised of a dielectric sandwiched between two metal plates. When a load was applied to the sensor, it would deflect the dielectric and change the distance between two plates. They calibrated the change in capacitance to the applied force. For better results, they fabricated the sensor with gold plates and parylene-C as the insulating material to address the biocompatibility and electrical properties like permittivity and resistivity. Using the MEMS technology, they miniaturized the sensor to fit in the small surface of a da Vinci Cadier™ grasper. Their results showed that the proposed capacitive force sensor could measure the dynamic and static force in the range of 0 to 40 N with a base capacitance of 16.3 pF for 1 mm^2 and 146 pF for 9 mm^2 capacitive area.

Recently, Kim *et al.* [37] proposed a novel sensorized surgical forceps comprised of two compact capacitive sensors on both jaws of the forceps. During a surgical procedure, forceps would undergo three manipulation forces in three directions due to pitching, yawing, and sliding. Also, rotational torque and grasping force are applied to the forceps by rolling and grasping motions, respectively [38]. In addition to that, the other surfaces were used to palpate the tissue by the surgeon to move or check tissue condition. To this end, two three-axis force sensors were designed to be installed at each jaw of the forceps to provide surgeons with all the forces and torque information. Each force sensor was composed of three perpendicular and parallel configuration of capacitance cells, a movable ground plate to convey the forces, and a triangular substrate. Fig. 9(a) shows the structure of each 3-DOF sensors under the load. The 3D design of the sensorized forceps and the prototype, manufactured by the machining process, are shown in Fig. 9(b) and Fig. 9(c), respectively. Utilizing a precise mobile platform and a pre-calibrated ATI-nano17 force sensor, they calibrated their 6-DOF sensors to 6-DOF external forces and torques on the grasper. The mapping equation was:

$$\begin{pmatrix} F_{grasping} \\ F_{palpation} \\ T_{rotation} \\ F_{manipulation-x} \\ F_{manipulation-y} \\ F_{manipulation-z} \end{pmatrix} = \begin{bmatrix} a_{11} & a_{12} & \cdots & \\ & \cdot & & \\ & & \cdot & \\ & \cdots & a_{56} & a_{66} \end{bmatrix} \begin{pmatrix} \Delta V_{cell-1} \\ \Delta V_{cell-2} \\ \Delta V_{cell-3} \\ \Delta V_{cell-4} \\ \Delta V_{cell-5} \\ \Delta V_{cell-6} \end{pmatrix}, \quad (8)$$

where, a_{ij} were the calibration constants and V_{cell-i} were the change in voltage of the $i-$th capacitive sensor (named as a sensing cell). The calibration constants were identified with applying known uni-axial forces on the grasper and performing a least square error fitting on (8). The verification experiments showed 3.2, 0.51, and 1.53 N for maximum manipulating forces in X, Y, and Z directions, respectively. Also, the maximum torque was measured 0.42 mNm. For this sensor, packaging the electronic components for sterilization was mentioned as a future development.

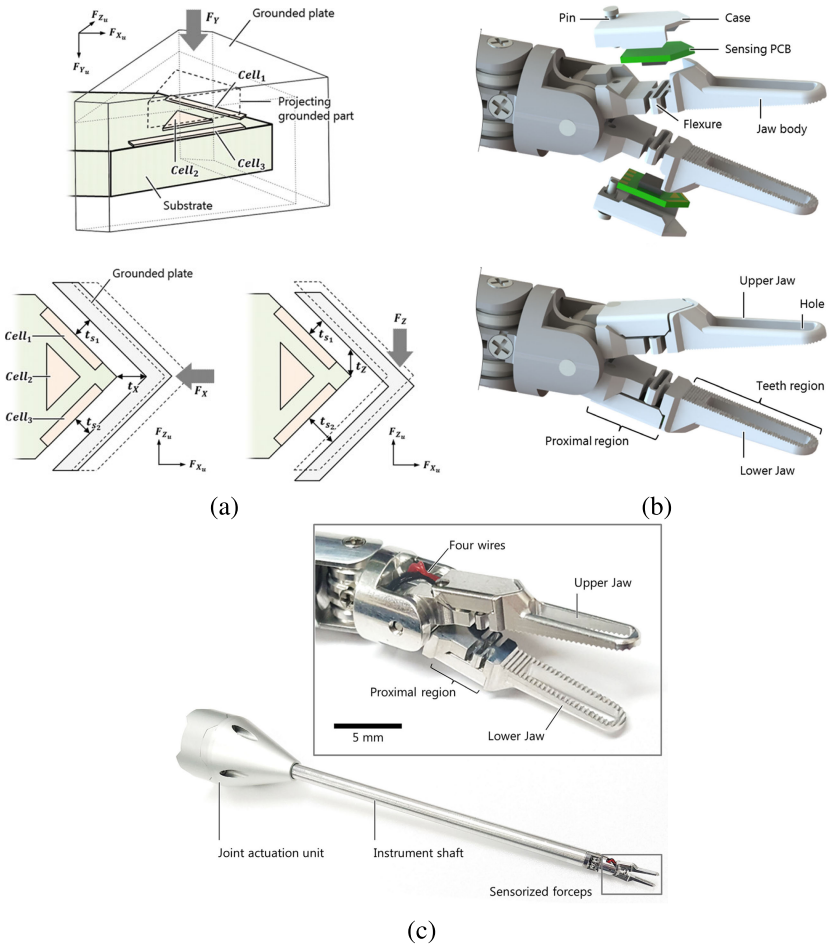

FIGURE 9. (a) structure of the capacitance cells on the substrate, (b) 3D design of the sensorized forceps, (c) micromachined prototype with an integrated sensor [37].

Capacitive tactile sensors are generally highly sensitive and precise. Such sensors typically have a force range of $0 - 20$ N with capacitance less than 1 pF. Also, relatively easy integration with MEMS technology to design thinner dielectric layers and having high resolution and temperature independence are the remarked advantages. These advantages make the capacitive tactile sensors favorable options for surgical tactile sensors [16], [36].

On the other hand, compromised repeatability due to the hysteresis and cross-talk has limited the use of the capacitive sensors for very high-precision applications. Also, electromagnetic interference with neural or cardiac activity has limited their use in the heart and brain surgery [6]. A summary of the most investigated capacitive tactile sensors in MIS is presented in Table 1.

B. OPTICAL-BASED TACTILE SENSORS

The contributions of optical tactile sensors in the MIS and RMIS applications are described in this section. The emphasis was on the sensors prototyped and validated in at least one physical or functional requirement for a tactile sensor in *in-vivo*, *in-vitro*, or *ex-vivo* experiments.

The first literature reporting development of an optical sensor for medical applications dates back to 1953s. The first application of such a sensor was intravascular and cardiac diagnostic measurements [39]–[41]. In 1960, Polanyi and Hehir [42] presented an optical system for the measurement of the *in-vivo* oxygen concentration in the blood. In an early study, Frommer *et al.* [43] proposed a fiber-optic catheter system that could record intracardiac oxygen saturation continuously up to 3 hours in the patients with valvular heart disease. Their instrument provided a novel and valuable tool both for cardiovascular diagnosis and clinical investigations.

During the years, numerous optical tactile sensors have been designed and introduced to be used in the medical approach, especially in MIS procedures. The main characteristics of the optical sensors, that led to their wide adoption in MIS were intrinsic small size, biocompatibility, magnetic, and electrical passivity. Thanks to these specifics, the development of optical tactile sensors for the MIS has gained momentum over the electrical-based sensors. Especially for MRI-guided surgeries such as the brain and cardiac interventions, the optical-based sensors have been the only MRI

TABLE 1. Summary of the representative studies on electrical-based tactile sensors in MIS.

Authors	Year	Principle	Application	Measurands	Range	Characteristics
Dargahi *et al.* [46]	2000	Piezoelectric	Endoscopy	Force	2 N	Error: 0.2 N
Eltaib *et al.* [34]	2000	Capacitive	Laparoscopy	Force	0-75 mV	Capacitance < 60 pF
Kattavenos*et al.* [47]	2004	Piezoresistive	MIS	Pressure	245-1080 kPa	N/A
Ottermo *et al.* [48]	2004	Piezoelectric	MIS	Force	10 N	$A_{profile}$=24×8 mm
Qasaimeh *et al.* [49]	2008	Piezoelectric	MIS	Force	0.01-4 N	Not Reported
Trejos *et al.* [50]	2009	Piezoresistive	MIS	Force/Torques	$F_{lateral} = \pm 5$ N $F_{axial} = \pm 25$ N $T_{rotation} = \pm 80$ Nmm	$RMSE_{force}$: 0.35 N $RMSE_{torque}$: 1.5 Nmm
Golpaygani *et al.* [51]	2009	Capacitive	RMIS	Force	0.1-0.7 N	Sensitivity: 0.83 kHz/N
Jalkanen *et al.* [52]	2010	Piezoelectric	Palpation	Stiffness	2-10 kPa	$R^2 = 0.94$, p < 0.05
Kalantari *et al.* [53]	2011	Piezoresistive	Catheterization	Force	0.1-2.5 N	RMSE: 0.611 N
Baki *et al.* [54]	2012	Piezoresistive	MIS	Force	2 N	Res_F: 5 mN
Talasaz *et al.* [55]	2012	Capacitive	Profilometry	Force	$F_{palpation}$=4-5 N $F_{gripping} = \pm 0.5$ N	N/A
Hwang *et al.* [56]	2013	Piezoresistive	RMIS	Force	0.0-3 N	Linearity > 99.6%
Lee *et al.* [57]	2014	Piezoelectric	Palpation	Force/Pressure	3-30 kPa	Sensitivity: 0.38 $^{mV}/_{kPa}$
Li *et al.* [58]	2015	Piezoresistive	MIS	Force	$F_{axial} = \pm 3.0$ N $F_{radial} = \pm 1.5$ N	Res_{axial}=0.15 N Res_{radial}=0.015 N
Kim *et al.* [59]	2015	Capacitive	MIS	Force	F_x=±2.5 N, F_y=±5 N F_z=±2.5 N, $F_{grasping}$= 5 N	$RMSE_x$=0.0837 N, $RMSE_y$=0.0732 N $RMSE_z$=0.114 N, $RMSE_{grasping}$=0.0957 N
Hessinger *et al.* [60]	2016	Piezoresistive	MIS	Forces/Torques	10 N 1 Nm	$Error_{axial}$= 4.92% $Error_{rotation}$= 1.13%
Zhang *et al.* [61]	2017	Piezoelectric	MIS	Tissue Hardness	< 500 kPa	N/A
Kim *et al.* [62]	2017	Capacitive	RMIS	Force/Torque	Force=±1.5 N $Torque_z$=±20 Nmm $Torque_{x,y}$=∓10 Nmm	Res_F=0.21 mN Res_T=0.35 Nmm
Rado *et al.* [63]	2018	Piezoresistive	MIS	Force	Gripping Force: 1-20 N Tactile Sensing:0.01-2 N	N/A
Ju *et al.* [64]	2019	Piezoelectric	Catheterization	Tissue Hardness	0-1.7 MPa	Errors < 3.5%
Kim *et al.* [65]	2020	Capacitive	RMIS	Force/Torque	F_x=±0.3 N, F_y=0-0.5 N F_z=0-0.9 N, $F_{gripping}$=0-0.9 N	Average Elastic Modulus, E =581 kPa Accuracy=98.1%

RMSE: root mean square error, R^2: goodness of fit, Res_F: force resolution, Res_T: torque resolution.

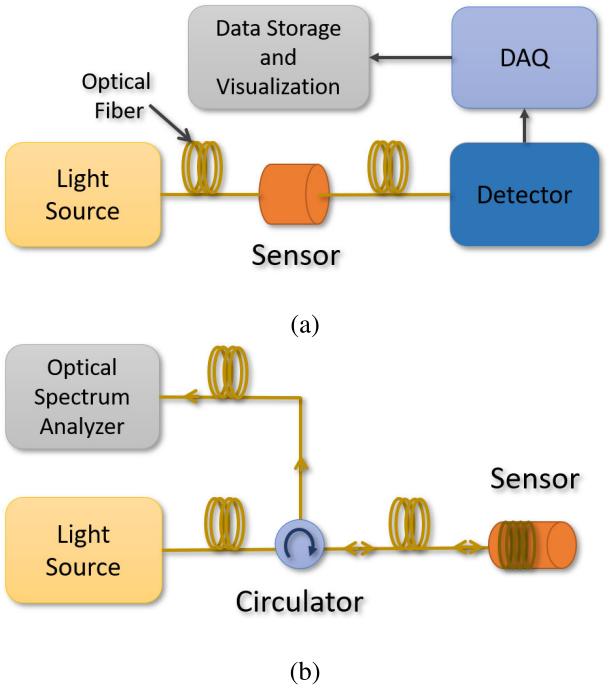

FIGURE 10. Typical system components of an optical sensor system based on (a) LIM principle, (b) WM and PM principles.

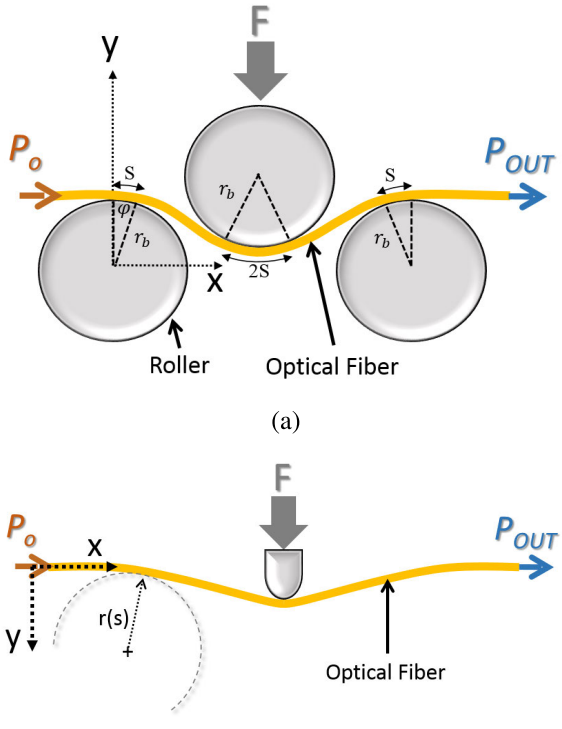

FIGURE 11. Bending loss configurations: (a) constant bending radius (CBR), (b) variable bending radius (VBR).

and electrically passive sensing modalities. The basic sensing element of optical tactile sensors is an optical fiber. The optical-fiber-based sensors mainly work based on three principles: wavelength (WM), phase (PM), and light intensity modulation (LIM) [6], [44], [45].

As depicted in Fig. 10(a), an optical fiber sensor system generally consists of a light source, to which an optical fiber is connected and the light is transmitted from the source into the optical fiber. The optical fiber is passed through the sensor structure, where the intensity, phase, or wavelength modulation happens. Afterward, the modulated light goes to an optical detector. The choice of the optical detector depends on the sensing principle, whereas, for intensity modulation, the detector could be a photodetector or a camera to measure the intensity of the passed (or reflected) light in the fiber. Also, the detector could be an optical spectrum analyzer (OSA) for obtaining the wavelength spectrum of the light, or a fringe-pattern display to quantify the phase modulation (Fig. 10(b)). A post-processing step is also required to obtain the calibration parameters after recording the output light.

1) LIGHT INTENSITY MODULATION OPTICAL TACTILE SENSOR

The first generation of the optical sensors was designed based on the intensity-modulation principle. This sensing principle relies on the variation in light power due to an external modulator parameters like force, pressure, displacement, temperature, etc. LIM sensing principle provides the unique advantages of being inexpensive, thermally insensitive, simple in design, and easily implementable. Thanks to these features, intensity-modulated sensors are favorable for making array sensors and multiple DoF sensors. The main modulation modes in the LIM sensing principle are bending loss and coupling loss. In continuation, these principles will be described and exemplified.

1) Bending Loss Principle When an optical fiber is bent along its length, the change in the incidence angle of the light beam causes intensity loss [66]. Theoretically, there is a critical bending radius for any fiber. When the bending radius is larger than the critical bend radius, there is no intensity loss, and when it is smaller than the critical bending radius, the intensity loss occurs. The critical bending radius is an essential factor for the sensor design. Fig. 11(a) schematically represented an optical fiber under a single-radius bending deformation induced by force, F.

   One of the most adopted theoretical models for the intensity modulation is presented in Fig. 11(a), which was first formulated by Gauthier, R.C. and Ross C. [66]. In their analysis, it was assumed that the fiber undergoes constant bending radius (CBR) deformation by passing through a mobile and two fixed cylindrical indenters (rollers). Applying the force on the upper mobile indenter bends the fiber and causes a light leakage from the body of fiber and intensity decay in the light output. The power decay model shows the correlation between the displacement of the mobile roller with the output power of the optical fiber. It has

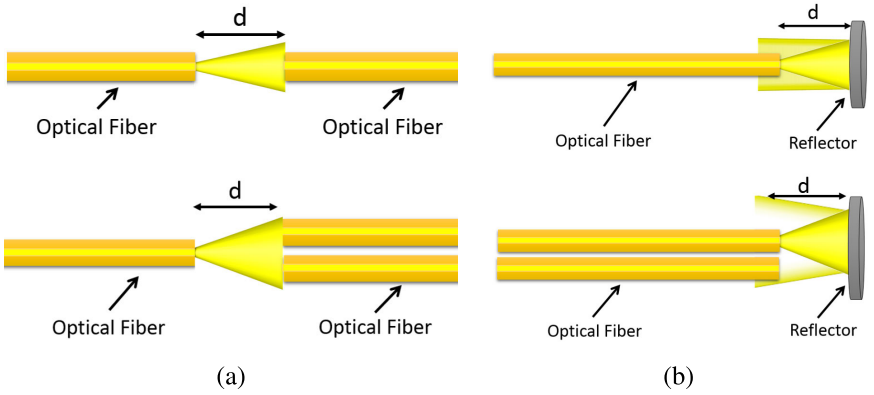

FIGURE 12. Optical fiber coupling loss configuration: (a) transmission loss, (b) reflection loss.

been used for calibration of the bending-based intensity modulation optical fiber tactile sensors. Equations (9)–11 express the relationship between the power loss and central curvature angle of in a constant bending radius deformation [66].

$$P(s) = P_0 e^{-\gamma s}, \tag{9}$$

$$s = r_b \varphi, \tag{10}$$

$$\gamma = c_\circ r(s)^{-\frac{1}{2}} e^{-c_1 r(s)}, \tag{11}$$

where, P_0 is the input power to a fiber with a constant bending radius of r_b and a curvature length of s; whereas $P(s)$ is the power at the desired length, s, on the fiber bent arc, and γ is the constant known as the bend loss coefficient. γ is an intrinsic constant dependent on the wavelength of the transmitting light, geometry, and optical characteristics of the fiber, e.g., critical angle, the refractive index of core and cladding.

Also, $r(s)$ is the local radius of curvature as a function of arc length of s and c_0 and c_1 are intrinsic optical properties of the fiber. Using two corrugated moving plates to apply a series of micro bending along the fiber length sandwiched between the plates, is another common type of bending loss optical sensors. In this configuration, multiple bendings cause more intensity loss and improve the sensitivity of the sensor [67].

The use of cylindrical rollers made the physics underlying the intensity modulation simple by enforcing a constant bending radius (CBR) configuration. However, it made the sensor structure bulky and was a limitation for the miniaturization. To cope with this limitation, Bandari *et al.* [13], [27] introduced a new sensing principle based on a variable bending radius (VBR). The VBR principle was based on utilizing only a single arbitrary shape indenter with a significantly small size. Fig. 11(b) depicts the VBR configuration. They formulated the VBR principle by differentiating (9) with respect to s. Their proposed formulation was based on integrating the infinitesimally small change in the power employing $d\gamma$ as:

$$dP(s) = (-\gamma P_0 e^{-\gamma s} - sP_0 e^{-\gamma s}(-\frac{1}{2} c_\circ r(s)^{-\frac{3}{2}} \times e^{-c_1 r(s)} - c_\circ c_1 r(s)^{-\frac{1}{2}} e^{-c_1 r(s)}) \frac{dr(s)}{ds}) ds. \tag{12}$$

By integrating the $dP(s)$ over the length of the fiber, the power-loss was obtained as a function of the radius of curvature function, $r(s)$, as (13).

$$\int_0^s dP = P(s) - P_0. \tag{13}$$

2) Coupling Loss Principle Coupling loss-based optical sensors work with two modalities: transmission loss and reflection loss. In both modalities, the light intensity is changed while it transfers between two coupled optical fibers. In the transmissive LIM sensors, typically, a gap between the fibers results in a predictable initial coupling power loss, which would change with the transverse, longitudinal, and angular misalignments between the fibers. Fig. 12(a) illustrates a schematic of transmission loss due to distance d, between two optical fibers.

Equation (14) states the fundamental model relating the coupling efficiency, η (the ratio of the transmitted power to the initial power) to the angular misalignment between the fibers, and the gap length [40].

$$\eta = \frac{P_{out}}{P_{in}} = 4\frac{D}{B} exp\left(-A\frac{C}{B}\right), \tag{14}$$

where A, B, C, and D are intrinsic properties of the fibers, structural design parameters, gap medium between the fibers and the angular misalignment caused by the physical load, respectively. Comparing the output (measured) and input powers (set at the source), the coupling efficiency, η is calculated, and the unknown parameters in (14), are estimated.

The second coupling loss principle is the reflective LIM, as shown in Fig. 12(b). In this configuration, a movable reflecting surface is placed in distance d in

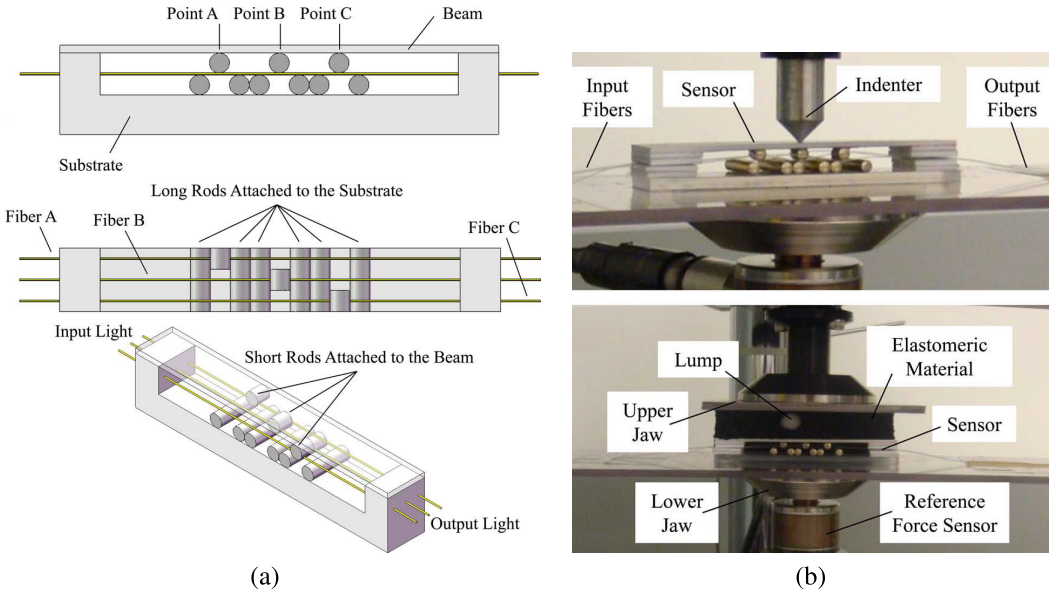

FIGURE 13. Bending loss tactile sensor proposed by Ahmadi *et al.* [70]: (a) structural design, (b) fabricated sensor under the point load and interaction with the tissue phantom.

front of the fibers perpendicular to their central axes. Most of such sensors have been proposed based on using a pair of straight parallel optical fibers, whereas one is the emitting fiber projecting light to the reflector, and one fiber receiving the back-scattered light. The intensity of the received light is proportional to d. For further simplification of the design, researchers have used a fiber-optic coupler to couple the reflective light to a single fiber, i.e., known as retro-reflective fiber.

Faria [68] presented a theoretical analysis of a reflective sensor with a pair of straight parallel optical fiber. In [68] geometrical approach and electromagnetic theory of the paraxial Gaussian beam approach revealed that the increase of the distance would initially increase the reflective light intensity while more distance would decrease the intensity. Polygerinos *et al.* [69] described a mathematical model for the fiber-optic reflective LIM sensor using an optical coupler. They used the Gaussian light-intensity distribution and modeled the transmitted light in two configurations, i.e., axially moving reflector and tilted reflector along the axis perpendicular to the optical fiber axis. They experimentally proved that the collected light was a function of the distance d.

There are several examples of LIM optical tactile sensor in the literature. For example, Ahmadi *et al.* [70] developed a bending loss optical tactile sensors composed of three single-mode optical fibers where each fiber passed trough three perpendicular rods. Each fiber was sandwiched between one short movable rod and two fixed rods. Three upper movable rods were attached to a flexible beam in certain different lengths. Fig. 13(a) shows the configuration of the rods and fibers in this sensor. The beam was glued in two sides to the sensor substrate. The applied force would deflect the beam, and the rod would bend the connected optical fiber. The bending caused intensity decay in the deformed optical fiber. Therefore, measuring the relative deflection of the beam resulted in estimating the unknown force.

They used silica sheets to fabricate the substrate sensor to achieve the biocompatibility and electrical passivity requirements. The beam was made of hi-impact polystyrene to have sufficient flexibility. The point load was applied on different locations on the beam while the intensity output was being recorded as the output voltage of the photodetectors.

The validation experiment was done by considering the interaction between an elastomeric tissue phantom consist of a rigid artificial spherical tumor. The fabricated sensor under the point load and interaction with the tissue phantom is depicted in Fig. 13(b). Results verified that the sensor was able to identify the location of the concentrated force caused by a rigid tumor. The range of measurement was demonstrated in 0-4 N. Furthermore, the sensor worked under both static and dynamic loading conditions. Also, they recommended using the MEMS technology to miniaturize the sensor structure and utilizing the micromirror to reflect the output light.

In continuation, Bandari *et al.* [71] proposed an array optical sensor to measure the lateral and circumferential force for valvuloplasty cardiac surgery. The proposed sensor was composed of four single VBR optical sensors that were configured cylindrically. Four semi-cylindrical indenter were attached to the inner surface of the flexible shell in different longitudinal locations. This configuration made the sensor integrable at the tip of a valvuloplasty catheter. A parametric finite element analysis was done to model the sensor. The analytical and numerical validation of the sensor provided the feasibility of using this sensor to consider the heart valves condition and location.

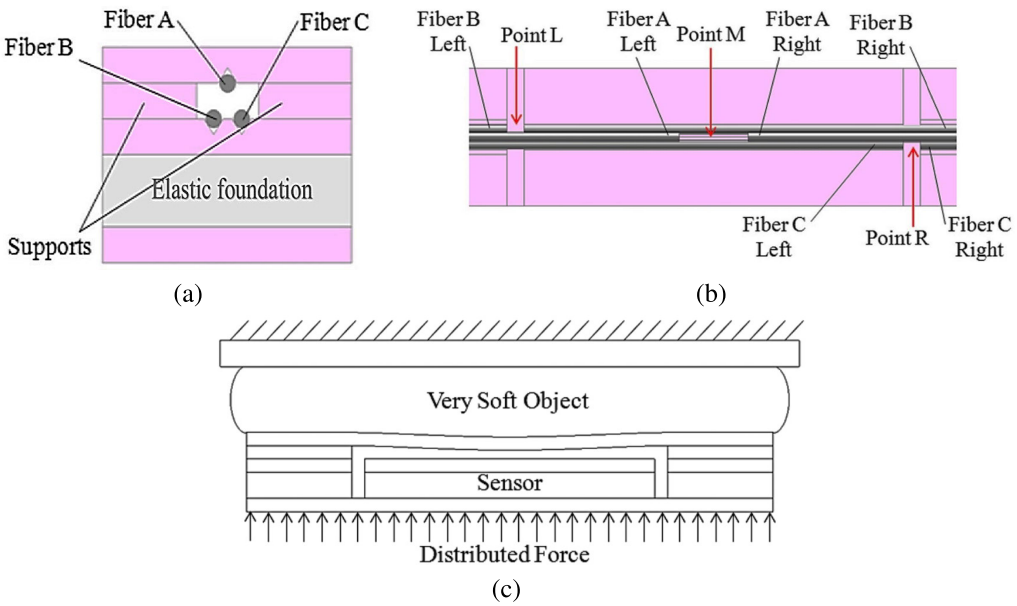

FIGURE 14. Proposed transmissive coupling loss optical fiber sensor by Ahmadi *et al.* [72]: (a) cross-sectional view of the structure of the sensor, (b) top view of the configuration of fibers and gaps, (c) illustrative presentation of typical deflection of sensor and soft tissue under distributed force.

In another study [72], a novel sensing mechanism was proposed, fabricated, tested, and shown to be feasible for MIS procedures (Fig. 14). The working principle of the proposed sensor was based on calculating the deformation of contacting tissue through measuring the transmissive coupling loss through a fiber attached to the top beam. Similarly, the total contact force was estimated by measuring the coupling loss through two receiving fibers. Quantitative estimation of the stiffness of the tissue was shown to be correlated to the ratio of force to the deflection. The coupling loss between the left and right portion of fiber A was due to the gap and angular misalignment. Deformation of tissue produced the angular misalignment of left and right portions of fiber A; while, the power loss at fibers B and C was due to both the gap and lateral misalignment. The lateral misalignments of left and right portions of fibers B and C were produced due to the deformation of the elastic foundation.

In this study [72], an N-Type < 100 > silicon wafer was used to make the beams, substrate, and supports while a PDMS film was used to make the elastic foundation. Three single-mode optical fibers were utilized and connected to three photodetectors to measure the transmitted light intensity. Also, an ElectroForce testing machine was used to apply the force on the tissue in two modes: a dynamic concentrated force to examine the response of the sensor under dynamic loads and a test with a distributed force to examine the ability of the sensor in lump location.

To verify the ability of the sensor in measuring the relative softness of different tissues, three silicon rubbers with different shore hardnesses were used. During the experiments, a force with a triangular function was applied at a frequency of 0.1Hz. The results verified that the proposed sensor was capable of distinguishing three distinct materials. Moreover, the results demonstrated equal outputs from both fibers B and C, which indicated a homogeneous distribution of force on the sensor. However, shape optimization was needed to address the miniaturization and waterproof requirements. In addition, a more detailed mechanical model (analytic or FEA) should be provided to investigate the sensitivity of the sensor to the size, depth, and material properties of the lump in the tissue during lump location applications.

As an emerging MIS approach in the last decade, cardiac surgery on a beating heart has been expanded significantly, i.e., the off-pump technique. MIS techniques have played a key role in this expansion. For example, mitral valve replacement (MVR) (and annuloplasty) was one of the first major cardiac surgeries which were revolutionized by catheter-based techniques (CBT). During a CB-MVR an artificial mitral valve is deployed on the defective natural valve using a metallic expandable anchorage device. To secure the prosthetic valve in place, on the annulus (peripheral ring of the valve), a minimum anchorage force of $1.5 - 4$ N is reported to be necessary upon deployment [73]. Conventionally, anchorage of the valve is examined manually and qualitatively by the surgeon; however, due to beating movement of the heart and valve motion, the tactile perception of the surgeon from the anchorage force is polluted.

Therefore, to address the need for a sensor capable of precise force measurement in the highly dynamic intracardiac environment, Yip *et al.* [74] developed an optical tactile sensor based on the reflective light intensity modulation principle. The proposed sensor was comprised of three pairs of

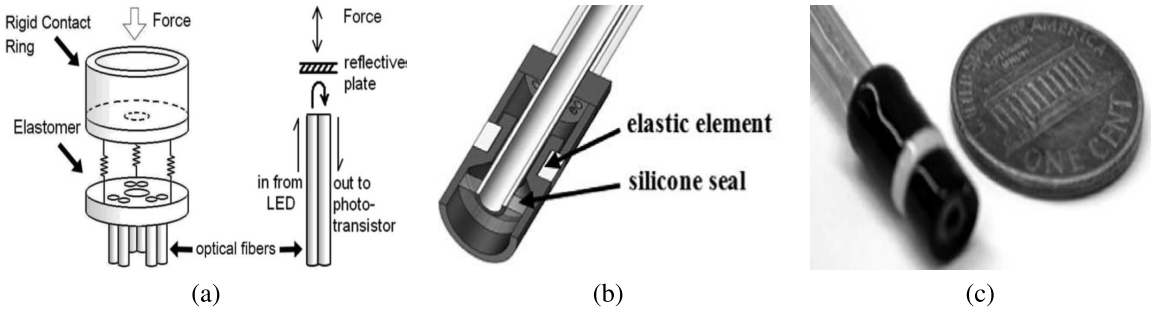

FIGURE 15. Reflective light intensity modulation tactile sensor proposed by Yip *et al.* [74]: (a) sensing principle of the sensor, (b) cross-sectional view of the sensor, and (c) fabricated prototype of the sensor.

optical fibers placed in a triangular configuration. Each pair of fibers included an emitting fiber, coupled to a light source, and a receiving fiber connected to a phototransistor circuit. A reflecting plate was located at a distance of 4 mm against the fibers. The external diameter and the length of the sensor were ϕ5.5 mm and 12 mm, respectively.

To avoid the interfering with the intra-operative ultrasonic imaging, the rigid components were made of acetal material. A silicon sealer provided fluid sealing of the sensor. An elastic component (Silicon rubber, Polysiloxane, with a shore hardness of 35) was used to join two parts of the sensor with flexibility. Upon applying a force on the tip of the sensor, it would press the elastic element and subsequently changed the orientation of the reflective plate. The change in the spatial orientation of the plate would cause depreciation of the light intensity in the receiving fiber. Fig. 15 illustrates the sensing principle, geometric design, and final prototype of the proposed sensor. Since Silicon rubbers exhibit a nonlinear force-deflection behavior with hysteresis; therefore, the quadratic viscoelastic function was used for calibration. The calibration was performed by applying a sinusoidal chirp force to the sensor, with an amplitude of 4 N and a terminal frequency of 6 Hz. To simulate the immersion of the sensor in blood, the calibration tests were performed in the water while its temperature was maintained at 37°C. In order to assess the generality of the obtained coefficients, the input loads of chirp waveform and triangular waveform were reconstructed from the voltage signals. The correlation coefficient of reconstruction and chirp input was $R^2 = 0.9889$ and for triangular input was $R^2 = 0.9867$. *In-vivo* experimentation on the sensor was performed on Yorkshire pigs. The sensor was integrated on a 14−guage needle and inserted into the left atrium of the animals. The tests were conducted under 3D ultrasound navigation.

During the surgery, surgeons had real-time visual force feedback and tried not to exceed the force magnitude of 1.5 N. Post-mortem examinations show that the anchor was deployed correctly in place with a force of less than 2 N. However, due to the integration of the sensor on a rigid surgical instrument, surgeons could perceive the force during the operation to control the required force magnitude, while in the case of robotic surgeries or flexible instruments, the transmitted light can be sensitive to optical fiber bending. Furthermore, the elastic component material properties should be considered due to hysteresis in higher frequency signals.

Another emerging field of MIS application is cardiac ablation. A common cardiovascular disease is the abnormal heart rhythm or cardiac arrhythmia [76]. During the years, different medication courses have been investigated for arrhythmias, yet the most effective treatment is the radiofrequency ablation surgery (RFA). During RFA, a long, thin, and flexible catheter is subcutaneously steered to the right atrium. By tracking the catheter tip via real-time fluoroscopic imaging, the surgeon confirms the secure contact between the RF electrode and the atrial wall and initiates the ablation process [10]. Studies have revealed that the electrode-tissue contact force is a major factor affecting the success of an RFA procedure. A large contact force, i.e., beyond 0.3 N, would tear or perforate the tissue, while an insufficient force leads to a suboptimal contact area and fail the procedure [15]. To satisfy these requirements during the ablation procedure, sensors are designed to be integrated at the tip of the catheter.

In this regard, Noh *et al.* [75] proposed a new miniature three-axis force sensor, which is integrable at the tip of the ablation catheter to measure the contact force. In their study, a novel sensing mechanism based on reflective coupling loss LIM principle and an unprecedented intensity estimation mechanism based on CCD camera utilization was proposed. As depicted in Fig. 16(a), the sensor consisted of a flexible cylindrical casing with a mounted mirror inside, a four-core bundle optical fiber, an LED light source, and a CCD camera (resolution 640×480, at 30 fps). The mirror was fixed on three cantilever arms at a 3×120° circular configuration. Upon application of external force to the sensor, the flexible tip of the sensor would deflect and so would each of three cantilever beams. The deflections would move the white plate to a new orientation.

As illustrated in Fig. 16(b), the light source illuminates the tip of the sensor through one of the fibers. The reflected light from the interior mirror was transmitted back to the CCD camera through three optical fibers. An image processing software was developed to estimate the light intensity in each of the three receiving optical fibers. The reflected light

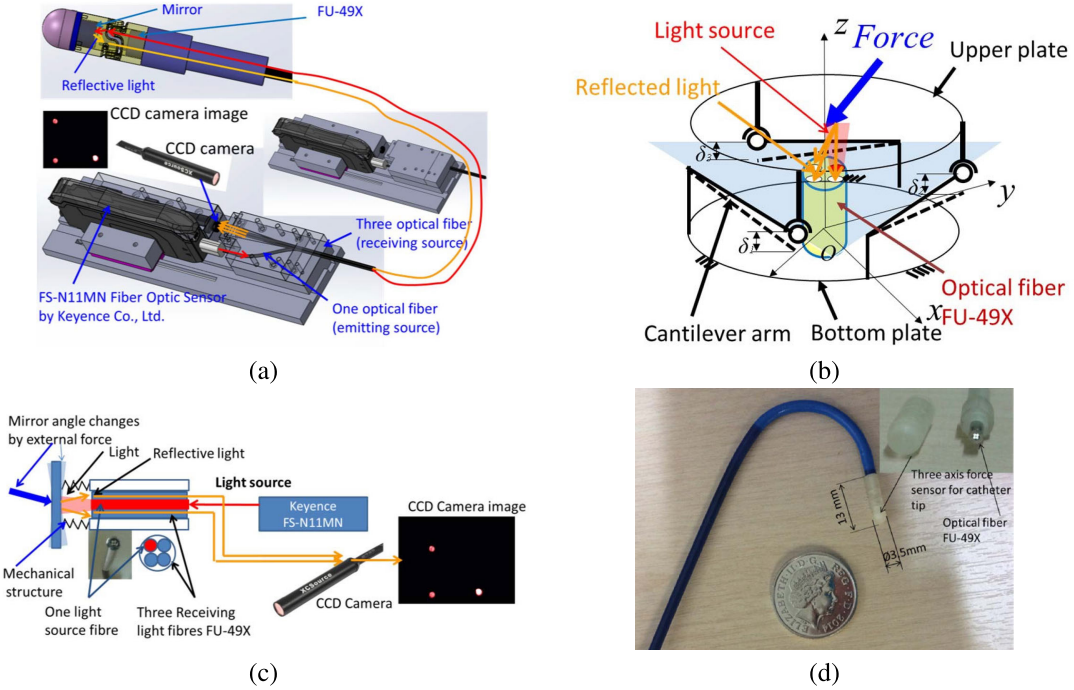

FIGURE 16. (a) schematic view of the sensor proposed by Noh *et al.* [75], (b) configuration of internal mirror and cantilever arms, (c) the image acquisition system, and (d) their prototyped sensor.

intensity is a function of the orientation of the mirror, and the deflection of beams governs the orientation. Since the deflection of a beam is linearly proportional to the force, the intensities of reflected lights recorded by CCD camera were mapped to the external calibration forces. To do so, a multi-linear regression model with nine-regression coefficients was used. As depicted in Fig. 16(c), each frame was divided into three regions of sections (ROS), which were corresponding to each fiber. The intensity value was calculated as the mean value of pixels in each ROS at a given time. The first prototype of the sensor consisted of a 3D printed deformable structure is shown in Fig. 16(d).

To perform the calibrations, a device equipped with a force sensor was used. The fabricated sensor was subjected to a compressive axial load of $F_z = 0$ to 1.5 N, and lateral push-pull forces of $F_x = F_y = -0.5$ to 0.5 N. Results showed a linear relationship between the light intensity values of three receiving fibers and the force applied to the sensor. However, this study could be further improved by increasing the resolution of the camera, implementing an edge detector over each ROS to discard the contribution of black pixels to improve sensitivity, studying the effects of filtering parameters on the accuracy, and re-configuring the bundle to be more symmetrical.

Intensity modulation optical sensors are popular for their inexpensive and simple sensing structure and processing system. They are not sensitive to temperature variation, thus, eliminates the need for a thermal compensation schema. On the other side, because of the light source fluctuation, fiber deflection in the bending model or fiber misalignment in the coupling loss model, there is undesired drift in the intensity data reading. A summary of the state-of-the-art of LIM optical tactile sensors proposed for MIS is tabulated in Table 2.

2) WAVELENGTH MODULATION OPTICAL TACTILE SENSOR

Wavelength modulation optical sensors were proposed to achieve higher resolution measurements in comparison with the LIM-sensors. For the first time, in 1978, Hill *et al.* [77] made a periodic change in the refractive index of the core of the optical fibers via electromagnetic waves and developed the Fiber Bragg Grating. Afterward, Meltz *et al.* [78] demonstrated a new method to develop Bragg grating in the fiber by exposure to coherent two-beam UV interference. An FGB-based sensor works based on the radiation reflection of a narrow range of wavelengths in the Bragg area on the core. The central wavelength of this range is called a Bragg wavelength, λ_B. Bragg wavelength is a function of the refractive index of the core, η_{eff} and the period of the grating, Λ, as expressed in (15):

$$\lambda_B = 2\Lambda\eta_{eff}, \tag{15}$$

Axial strain induced by physical loads like force, pressure, displacement, vibration, or temperature changes influences Λ and η_{eff}; thus, subsequently causes a reflected wavelength shift. The wavelength shift is defined as $\Delta\lambda_B$ and is calculated by (16):

$$\frac{\Delta\lambda_B}{\lambda_B} = k_\epsilon.\epsilon + k_T\Delta T, \tag{16}$$

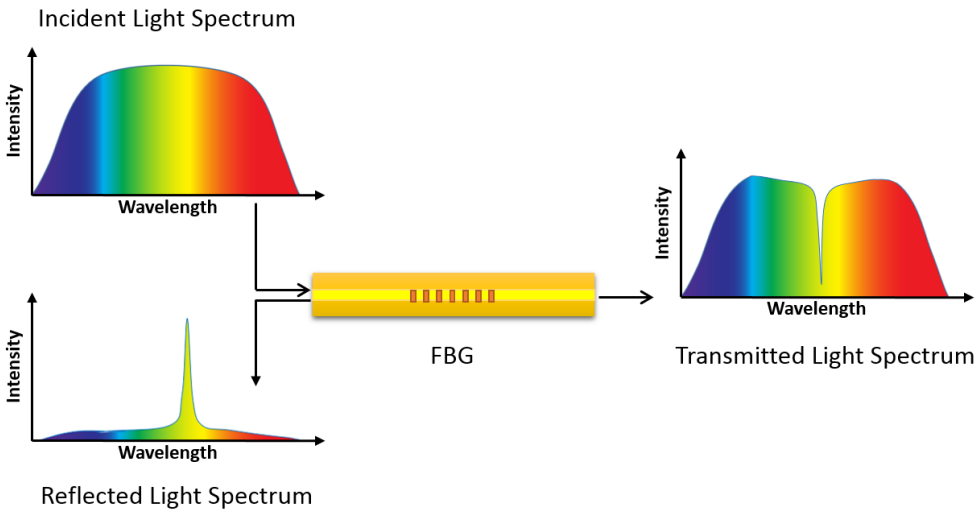

FIGURE 17. Sensing principle of the fiber Bragg grating and wavelength shift due to an axial strain.

where, k_ϵ is the coefficient for axial strain, ϵ and k_T is the coefficient for the temperature change, ΔT [79]. Depending on the application, a sensor structure is designed to translate the physical stimulus, i.e., force, pressure, thermal strain to FBG fiber. Afterward, calibration of the wavelength change with respect to the physical stimulus is performed the least square fitting. Fig. 17 schematically shows the input and output light spectra happening in a fiber Bragg grating due to an axial strain.

As a commercialized example, Yokoyama *et al.* [15] developed an FBG force sensor to be integrated at the tip of the RF ablation catheter. The sensor consisted of three FBGs embedded in a compliant tip of the catheter. During the ablation procedure, the contact force between the cardiac wall and the tip of the catheter caused axial strains and shifts on the reflected spectra of the three FBGs. Depending on the level of axial and lateral components of the tip force, each fiber would exhibit different spectrum changes. To validate the sensor, the researchers performed a total of 1409 measurements on two catheters in perpendicular, parallel, and 45° directions. Calibration was performed using a least-square error fitting. Afterward, the sensor was embedded in an RF ablation catheter and was used in 10 anesthetized canine animal models. The results confirmed the measurement linearity of the sensor with $R^2 = 0.988$. The mean error of readings was less than 1.0%, and the range of measurement was $0 - 0.5$ N with a resolution 10 mN. This sensor was later commercialized as a part of the ablation catheter TactiCath™ Quartz ablation catheter (formerly Endosense SA, Switzerland, acquired by Abbott Laboratories, Illinois, USA.) Fig. 18 shows the schematic of this sensor and the tip contact force during the ablation procedure.

In another representative study, Park *et al.* [79] proposed an MRI-compatible biopsy needle equipped with tactile sensors to measure the needle deflection profile while inserted into a tissue. In diagnostic biopsy and localized treatment monitoring, the tip of the needle is important to end up at the pre-planned location for taking biopsy samples. To this end, three optical fibers were attached to the inner part of the biopsy needle. The three FBG fibers were embedded in a circular pattern with 120° angular separations. Electrical discharge machining (EDM) was used to manufacture the

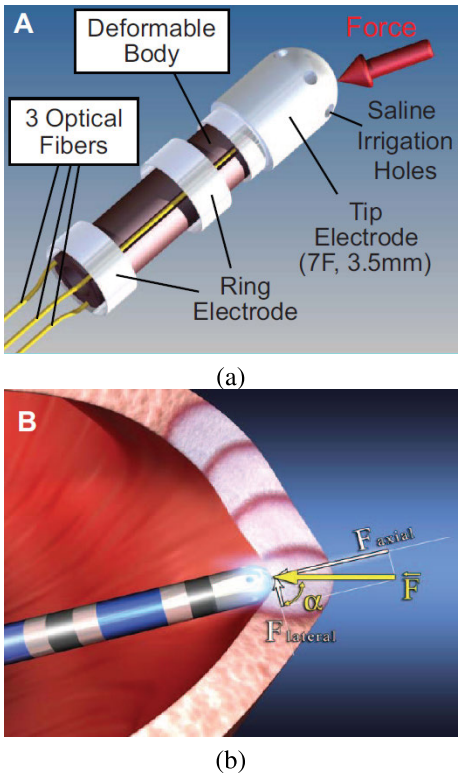

FIGURE 18. (a) schematic of the structure of the proposed sensor by [15], (b) reaction force on the catheter tip during the ablation procedure.

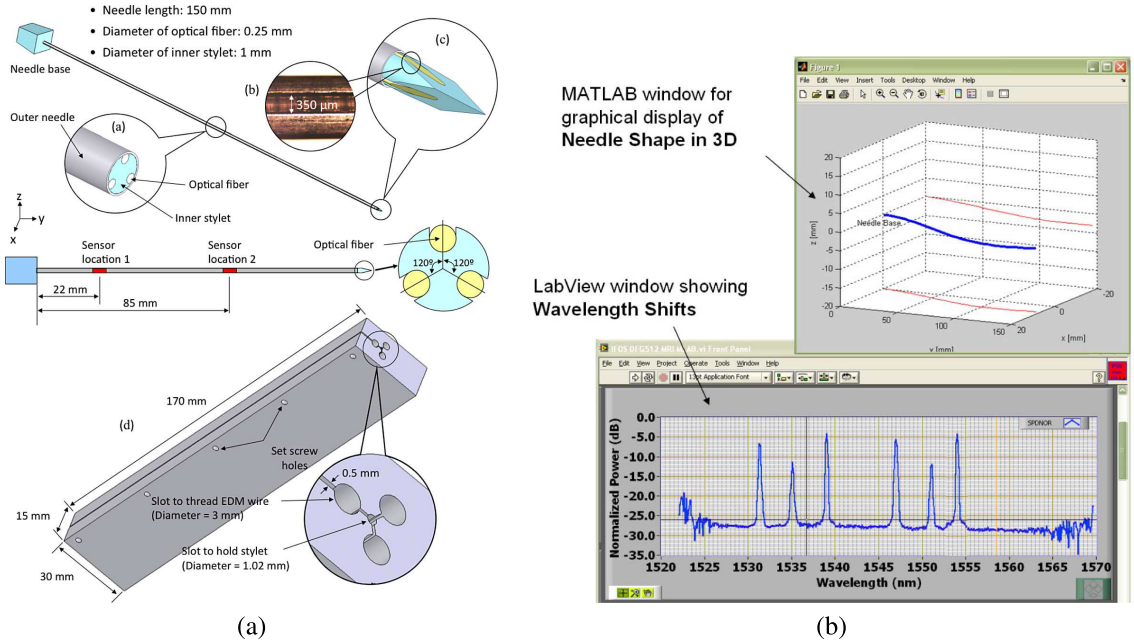

FIGURE 19. (a) sensor design with three fibers in a biopsy needle developed by Park *et al.*in [79], and (b) graphical display showing the shape of the needle and the wavelength shift.

fiber holder grooves in the needle. It helped to make accurate details in the metal without ferromagnetic extra parts to save MRI-compatibility. Fig. 19(a) illustrates the sensor designed with three fibers configuration in the biopsy needle and FBG locations.

The prototype was calibrated using two orthogonal digital cameras. The cameras were used to capture the 3D shape of the needle in bench tests. Calibration was done while needle deformed vertically and horizontally in lateral axes. Also, the needle was exposed to various temperatures in the range of $20°C$ to $55°C$ in the absence of any mechanical force. The researchers successfully mapped a linear transformation between the needle curvatures in two lateral axes and temperature change to the FBG wavelength shift. Fig. 19(b) shows a representative shape of the needle and its corresponding wavelength spectrum in bench tests.

Also, the needle was used under MRI imaging. Results showed fair agreement and verified accurate sensor performance in the MR environment. Using three or more fibers have been recommended to improve the system accuracy as well as using the sensors as force gauges to fine the tissue deformation model. This study shows a good example of sensor embedded medical devices for shape sensing flexible interventional instruments. Further development on this sensor could possibly be applicable for prostate and breast robot-assisted brachytherapy research [80], [81].

Zarrin *et al.* [82] developed two sterilizable sensorized needle driver graspers for laparoscopic instruments. Two FBG sensors were mounted in the custom-designed jaws of a grasper to measure axial and grasping force intraoperatively. The first prototype was designed with a T-shaped movable component contained an FBG to measure the axial force due to generated axial strain. A second FBG was attached to the working part of the jaw to capture the grasping force directly. Calibration was done to find the relationship between the reference force from an ATI-nano commercial force/torque (F/T) sensor and wavelength shifts of the FBGs. However, the first design was not reliable enough to measure the axial force because of the outward bending of the jaws while grasping an object. Also, the sensor was not capable of measuring the accurate force values in different locations on the jaw. Nevertheless, the sterilization and resolution requirements were not addressed [83]. To cope with the limitations, a new prototype was developed to improve the sensing ability. Due to achieve biocompatibility and sterilizability, stainless steel was used to manufacture the sensor structure. The jaw was fabricated using a wire EDM machine to have a high-quality surface finishing and resulted in less friction between the sliding parts, thus more accuracy of axial force measurement. An I-beam component was embedded in the second prototype, and two FBGs were attached to measure the axial and grasping force. To alleviate the undesired outward bending of the axial sensor, it was located at the neutral axes of the cross-section of the jaw for better reinforcement. In addition, an I-beam was attached at the tip of the instrument to reduce the axial strain. Fig. 20 depicts the sensor-embedded needle-driver grasper. Researchers utilized finite element analysis to predict the results deformation under working loads which were reported in acceptable axial strain and out-of-plane warping.

An optical interrogator was used to record the FBG wavelength, while the applied grasping and axial force were

TABLE 2. Summary of the representative studies proposing tactile sensors for MIS or RMIS based on optical sensing principles.

Authors	Year	Principle	Application	Measurands	Range	Characteristics
Webb *et al.* [95]	2000	FBG	MIS	Temperature	0-55 C	Res= $0.2^{\circ}C$ Error_{max}= $3^{\circ}C$
Tada *et al.* [96]	2002	LIM	MIS	Force	0-16 N	Res= 0.5 N Error= $\pm$0.3 N
Chapuist *et al.* [97]	2004	LIM	Neuroscience	Torque	$\pm$5 Nm	Res= 0.07 Nm S = 7.21 V/Nm
Su *et al.* [98]	2009	LIM	Biopsy	Force	0-20 N	Res= 0.2 N Linearity= 96.7%
Muller *et al.* [99]	2009	FBG	RMIS	Force	F_x=0-10 N F_y=0-10 N F_z=0-20 N	$\text{Res}_{x,y,z}$= 100 mN SD= 4 mN
Polygerinos *et al.* [100]	2009	LIM	Cardiac ablation	Force	0-1.10N	Res= 0.04 N Variation < 0.2 N
Kesner *et al.* [101]	2011	LIM	MIS	Force	0-10N	Res= 0.2 N RMSE <0.2
Su *et al.* [86]	2011	FPI	Needle steering	Force	10 N	Res= 1 mN SNR = 98%
Liu *et al.* [102]	2012	FPI	Eye surgery	Force	6 mN	Res= 0.25 mN S= 40 nm/mN
Polygerinos *et al.* [103]	2013	LIM	Cardiac ablation	Force	0-0.50 N	Res < 0.01 N Accuracy= 94% Linearity= 96% Hysteresis= 6%
Elayaperumalu *et al.* [104]	2014	FBG	Biopsy	Force	$\pm$0.5 N	Res= 0.043 N Error_x= 1.1 mN Error_y= 0.4 mN Error_z= 1.2 mN
Ahmadi *et al.* [105]	2015	LIM	MIS	Force	0-2N	Error=3%
Mo *et al.* [106]	2015	FPI	MIS	Force	0-5 N	Res= 0.1 mN
Qiu *et al.* [107]	2016	FPI	OCT	Force	1.2 N	Res= 0.25 mN
Li *et al.* [108]	2018	FBG	Palpation	Force	0-5 N	Res= 93 mN Error <8.22% Location< 8 mm
Bandari *et al.* [27]	2019	LIM	MIS	Grasping	0-2N	Res=0.02 N Linearity=94% RMSE=0.11 N SD=0.07N
Wanninayake *et al.* [109]	2019	LIM	MIS	Indentation	1-3 mm	N/A

S: Sensitivity, *SD*: Standard Deviation, *Res*: Resolution, *SNR*: Signal-to-Noise Ratio
OCT: Optical Coherence Tomography

recorded by ATI-nano F/T sensor. Furthermore, the location of the force was changed to evaluate the sensor response versus the location. The relationship between the recorded force data and FBG wavelength shift was calibrated using the linear regression. With the applied force in the range of $0-10$ N, the demonstrated measurement range of the sensor was $0-6$ N for grasping and 0.27 and 0.3 for loading along the $x-$, and $y-$ directions, respectively. The sensitivity for the grasping and axial sensors were 64.38 and 166.5 N/mm, respectively. The results were acceptable to present this sensorized needle-driver grasper for MIS applications. However, temperature compensation was still unmet.

In summary, the FBG-based sensors are bio- and MRI-compatible, which are the most limiting factor for non-optical sensing principles. Depending on the structural design and manufacturing material, the sensor could be sterilizable and physically robust. In addition, multiple FBG portion with various brag-lengths can be created along a single optical fiber and be calibrated to measure various parameters, simultaneously. Furthermore, due to their small size and flexibility, an FBG-based sensor can fit on the typically confined structures of surgical instruments used for MIS and RMIS applications. These sensors are sensitive enough to capture the small strain in the micro-scale. However,

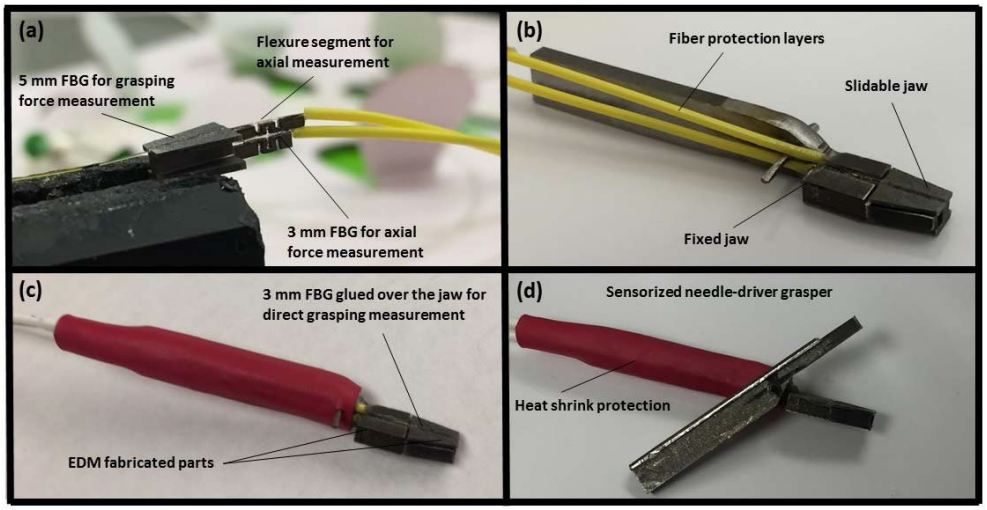

FIGURE 20. Two-DoF sensorized needle driving grasper equipped with an FPG sensor developed by Zarrin *et al.* in [82].

relatively expensive and sophisticated optical source and optical interrogator are needed for the FBG signal processing system. Also, a major drawback of the FBG sensors is that such sensors are intrinsically temperature-sensitive and require temperature compensation to preserve their sensitivity and accuracy. Nevertheless, FBG-sensors make favorable options for accurate temperature monitoring applications. Some MIS and RMIS application such as cryosurgery and radiofrequency tissue ablation [84] are associated with intraoperative high-temperature changes, e.g., from $-80°C$ to $+60°C$. Therefore, there is a compromise between the reliable range of working temperature and force sensing capabilities of FBG-sensors. Representative FBG sensors for MIS applications are summarized in Table 2.

3) PHASE MODULATION OPTICAL TACTILE SENSOR

Another optical phenomenon based on which sensors have been proposed is the phase modulation principle. Such sensors basically, work based on Fabry-Perot interferometry (FPI). The FPI-based sensors are comprised of a semi-reflective surface at the end of an emitting optical fiber and another (semi-)reflective surface place at a certain distance in front of it (Fig. 21). Such configuration is known as the Fabry-Perot cavity.

In a Fabry-Perot cavity, light reflects back partially to the emitting fiber, while another retro-reflection happens at the surface of the reflective surface at a distance. By visualizing the superposed light-emitting back from the fiber, circular infringement patterns form as a result of the phase difference between the two retro-reflections (one from the semi-reflective end of the fiber and one from the reflective surface in the cavity. By analyzing the width of dark and bright bands in the infringement pattern, a precise estimation of the distance (cavity length) is obtained. The band thickness and their intensity is a function of the Fabry-Perot cavity length; therefore, external force, pressure, and displacement causing the change in cavity distance can be calibrated with respect to the phase shift or change in the intensity of the fringes [86]. Depending on whether the light leaves the emitting Fabry-Perot fiber or reflects internally, this sensing principle is categorized as extrinsic and intrinsic, respectively. Fig. 21 depicts these two categories schematically. Also, a comprehensive review of the physics and application of FPI sensors is provided in [87]. Fig. 21 depicts both configurations of FPI sensors. The phase difference of the interference signal, δ_{FPI} is expressed as (17), [88]:

$$\delta_{FPI} = \frac{2\pi n^2}{\lambda} L_{cavity}, \tag{17}$$

where, λ is the wavelength of the incident light, n is the refractive index of the cavity main and L_{cavity} is the length of the FP cavity. In addition, the reflected intensity can be calculated through the summation of two reflected light intensity, I_1, I_2 with two different phases, ϕ_1, ϕ_2 and applying Euler's identity, (18), [89]:

$$I = I_1 + I_2 + 2I_1 I_2 cos(\phi_1 - \phi_2). \tag{18}$$

Shang *et al.* [85] proposed an MRI-compatible FPI optical sensor to measure needle insertion force for prostate cancer brachytherapy. They designed a mechanical fixture to keep the FPI sensor and embedded it into an MRI-compatible prostate needle insertion robot [90]. The sensing principle of the sensor and its structure are shown in Fig. 22(a). As illustrated, the fringes generated by red beams would be different from those created by black beams when the cavity length was changed by applying the load. Therefore, the change in fringe intensity was calibrated versus the magnitude of the applied force.

Also, a finite element analysis was performed for structural optimization to keep the sensor structure intact under the working force range. Calibration was done by putting

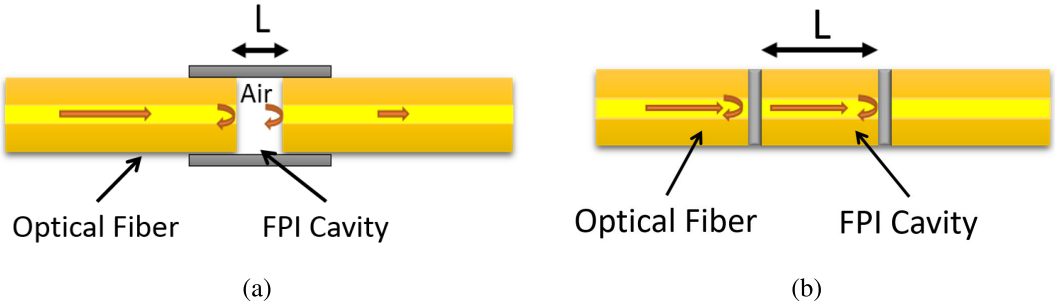

FIGURE 21. Fabry-Perot configuration: (a) extrinsic and (b) intrinsic.

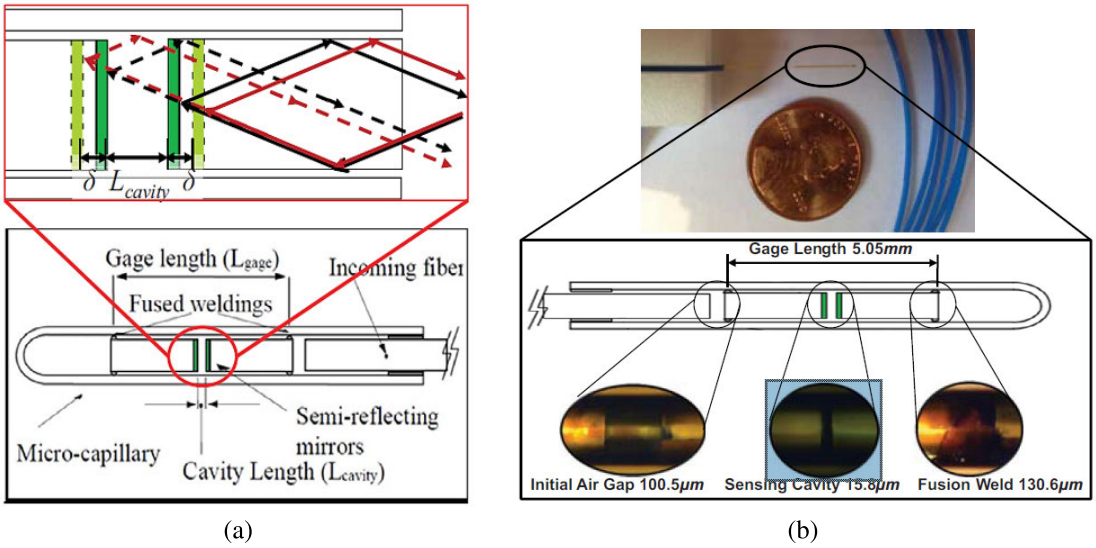

FIGURE 22. (a) structure and sensing principle of the FPI sensor proposed by Shang *et al.*in [85], and (b) their prototyped sensor embedded on a biopsy needle.

standard weights on the sensor prototype. Fig. 22(b) illustrate the FPI sensor in the biopsy needle. A photodetector converted the reflected light signal into a voltage signal, and force-voltage data were recorded for post-processing. The sensor worked accurately in the range of $0-10$ N with the 0.318 N root-mean-square (RMS-) error.

In another effort, Mo *et al.* [91] presented an FPI force sensing system to use in the needle insertion application. Two FPI sensors were mounted in parallel at the tip of a puncture needle with 1.54 mm internal diameter. The two sensors worked based on the interferometric intensity-phase modulation. One of the FPI sensors was designed to measure the axial force at the tip and temperature, while the second FPI sensor was utilized as the reference temperature sensor. The schematic figure of the two FPI sensors inside the needle tip and the sensor-embedded needle is shown in Fig. 23(a). A laser source with the wavelength 1550 nm transmitted the light and a splitter, which divided the light into two fibers. The interfered pattern of two sensors was measured by photodiodes, and the force and temperature estimation was performed in a computer workstation. Fig. 23(b) illustrates the temperature FPI sensor embedded on the needle.

The system was calibrated with a commercial dynamic force sensor and a linear model was obtained between the dynamic force and temperature compensated intensity phase of the FPI force sensor. The result showed that the system performance was accurate in the range of $0-8$ N and the temperature range of $23-37.5°$C. The system performance was verified with an insertion experiment inside a skin phantom at various temperatures and different insertion depths. Analyzing the tip force and insertion speed was recommended to detect the tissue type and its abnormality in the future investigation.

FPI sensors are highly sensitive with a tunable range of measurements. Structural optimization has become a scheme in fine-tuning FPI sensors for the mechanical requirements of MIS applications. Furthermore, FPI sensors can be integrated into the small space of the surgical instruments. Also, they are biocompatible and work in magnetic field environments properly. In comparison with the expensive optical analyzer of FBG sensors, signal processing of the FPI sensors is

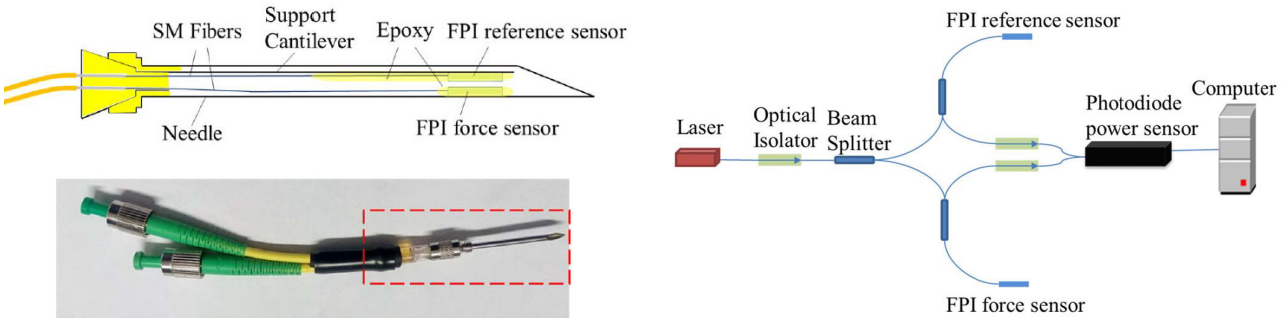

FIGURE 23. (a) schematic of the two FPI sensor inside the needle tip and the sensorized needle proposed in [91], (b) temperature compensation FPI sensor for MIS needle.

fairly simpler and does not require intense signal processing algorithms.

In addition, FPI sensors are sterilizable with both ethylene oxide and steam. However, care must be taken in handling these sensors, since the precise alignment and packaging of the fibers are crucial for maintaining the calibration. Another limitation of FPI sensors is that FPI cavities are intrinsically open structures, which firstly makes the whole structure of the sensor compliant and prone to fracture, and secondly makes it open to biological fluids. The latter would compromise the whole sensor performance by altering the light path, if not blocking. Also, the open cavity structure makes the sterilization validation process cumbersome due to providing a space for the micro-organisms to grow and not reachable by sterilizing agents [92]–[94]. Another limitation of the FPI sensors is manufacturability. Table 2 presents a summary of various FPI sensors developed for MIS applications.

IV. CONCLUSION

In this paper, articles proposing novel tactile sensors for MIS or RMIS application were reviewed. The main motivation for this paper was the lack of a multi-disciplinary review with the focus on tactile sensors with MIS/RMIS application. Most of the reviews in the literature are centered on the sensing principles, while some focus merely on artificial skin and artificial sense of touch for robots. Therefore, initially, a systematic categorization of the available sensors in the literature was provided, i.e., electrical-based and optical-based sensors. Afterward, the sensing principles and theoretical backgrounds, as well as the methodological details and technical advancements adopted by researchers in each category, were reviewed. At the end of each sensing principle, the representative studies were reviewed critically, and at last, the advantages and limitations of each were discussed.

An emerging research and development trend in the literature is the evolution of *hybrid* sensors. Hybrid sensors are basically, the sensors which employ more than merely one sensing principle to measure one or multiple physical stimuli, e.g., force, displacement, stiffness, etc. In fact researchers have proposed the use of hybrid sensors on two grounds: 1) for obtaining more robust measurements of physical stimuli, e.g., common noise cancellation, temperature compensation, and 2) for covering wider working environments, e.g., using a sensor under static forces and another under dynamic forces, or using a sensor when the magnetic field is present and another when the magnetic field is negligible.

There is a relatively small number of recent developments of hybrid sensors for MIS and RMIS, e.g., [110]–[117]. However, thanks to the adoption of the recently developed concepts of sensor fusion and machine learning, this field of research has gained momentum. There are still technical and methodological challenges such as multi-sensor cross-talk, noise amplification, heterogenous refresh-rate, asynchrony of sensor readings, and increased the complexity of the system. Therefore, new research efforts are yet expected to overcome the impediment of the technological limitations for hybrid tactile sensors.

Although the majority of the current literature has used a linear uni- or multi-variable regression calibration schema, new non-linear technique is emerging. Some of the recent developments have adopted more complex phenomena or structures such as variable bending radius (VBR) intensity modulation [13], [14] and viscoelastic structures [75] to achieve more precision and less hysteresis. Such phenomena or structures are intrinsically non-linear, thus need non-linear regression models. The models proposed include both analytical and heuristic models. While for analytical models, power-law and polynomial expressions have been the most popular, the heuristic models have adopted neural network [118], deep-learning [119], and support vector regression methods [6], [13].

In addition, the future works might include chamberless light modulation, rigorous modeling of the light modulation, rate-dependent calibration law, power spectral density analysis to quantize dynamics of the problem, camera-based intensity quantization, and miniaturization by using pre-bundled multi-core optical fibers. Also, as the shape-sensing of the soft-robots, e.g., catheters, for MIS and RMIS, has gained momentum in the field of robotics [7], [118]–[121], the need

for the body-embedded sensor for shape sensing is eminent and prominent.

ACKNOWLEDGMENT

The authors would like to thank the Natural Science and Engineering Council (NSERC) of Canada, the Fond du Recherche Nature et Technologie (FRQNT) of Quebec, and Concordia University for their support.

REFERENCES

[1] U. Seibold, B. Kubler, and G. Hirzinger, "Prototype of instrument for minimally invasive surgery with 6-axis force sensing capability," in *Proc. IEEE Int. Conf. Robot. Autom.*, Jan. 2006, pp. 496–501.

[2] A. M. Okamura, "Haptic feedback in robot-assisted minimally invasive surgery," *Current Opinion Urol.*, vol. 19, no. 1, pp. 102–107, Jan. 2009.

[3] S. Schostek, M. O. Schurr, and G. F. Buess, "Review on aspects of artificial tactile feedback in laparoscopic surgery," *Med. Eng. Phys.*, vol. 31, no. 8, pp. 887–898, Oct. 2009.

[4] T. Jaschinski, C. G. Mosch, M. Eikermann, E. A. Neugebauer, and S. Sauerland, "Laparoscopic versus open surgery for suspected appendicitis," *Cochrane Database Systematic Rev.*, vol. 11, no. 11, pp. 1–63, 2018.

[5] D. Vyas and S. Cronin, "Peer review and surgical innovation: Robotic surgery and its hurdles," *Amer. J. Robot. Surg.*, vol. 2, no. 1, pp. 39–44, Dec. 2015.

[6] A. Hooshiar, S. Najarian, and J. Dargahi, "Haptic telerobotic cardiovascular intervention: A review of approaches, methods, and future perspectives," *IEEE Rev. Biomed. Eng.*, to be published.

[7] A. Hooshiar, M. Razban, N. M. Bandari, and J. Dargahi, "Sensing principle for real-time characterization of viscoelasticity in the beating myocardial tissue," in *Proc. IEEE Int. Conf. Comput. Intell. Virtual Environ. Meas. Syst. Appl. (CIVEMSA)*, Jun. 2017, pp. 72–77.

[8] J. Stoll and P. Dupont, "Force control for grasping soft tissue," in *Proc. IEEE Int. Conf. Robot. Autom.*, Orlando, FL, USA, May 2006, pp. 15–19.

[9] P. Puangmali, K. Althoefer, L. D. Seneviratne, D. Murphy, and P. Dasgupta, "State-of-the-art in force and tactile sensing for minimally invasive surgery," *IEEE Sensors J.*, vol. 8, no. 4, pp. 371–381, Apr. 2008.

[10] P. Polygerinos, D. Zbyszewski, T. Schaeffter, R. Razavi, L. D. Seneviratne, and K. Althoefer, "MRI–compatible fiber–optic force sensors for catheterization procedures," *IEEE Sensors J.*, vol. 10, no. 10, pp. 1598–1608, Oct. 2010.

[11] A. S. Sezen, R. Rajamani, D. Morrow, K. R. Kaufman, and B. K. Gilbert, "An Ultraminiature MEMS pressure sensor with high sensitivity for measurement of intramuscular pressure (IMP) in patients with neuromuscular diseases," *J. Med. Devices*, vol. 3, no. 3, Sep. 2009, Art. no. 031006.

[12] R. Ahmadi, M. Packirisamy, and J. Dargahi, "High sensitive force sensing based on the optical fiber coupling loss," *J. Med. Devices*, vol. 7, no. 1, Mar. 2013, Art. no. 011001.

[13] N. Bandari, J. Dargahi, and M. Packirisamy, "Miniaturized optical force sensor for minimally invasive surgery with learning-based nonlinear calibration," *IEEE Sensors J.*, to be published.

[14] N. M. Bandari, A. Hooshair, M. Packirisamy, and J. Dargahi, "Bending-based formulation of light intensity modulation for miniaturization of optical tactile sensors," in *Proc. Opt. Sensors Opt. Soc. Amer.*,, Jul. 2018, pp. 1–2, Paper SeM2E–3.

[15] K. Yokoyama, H. Nakagawa, D. C. Shah, H. Lambert, G. Leo, N. Aeby, A. Ikeda, J. V. Pitha, T. Sharma, R. Lazzara, and W. M. Jackman, "Novel contact force sensor incorporated in irrigated radiofrequency ablation catheter predicts lesion size and incidence of steam pop and thrombus," *Circ. Arrhythm. Electrophysiol.*, vol. 1, no. 5, pp. 354–362, Dec. 2008.

[16] S. Stassi, V. Cauda, G. Canavese, and C. Pirri, "Flexible tactile sensing based on piezoresistive composites: A review," *Sensors*, vol. 14, no. 3, pp. 5296–5332, Mar. 2014.

[17] C. Chi, X. Sun, N. Xue, T. Li, and C. Liu, "Recent progress in technologies for tactile sensors," *Sensors*, vol. 18, no. 4, p. 948, Mar. 2018.

[18] J. Dargahi and S. Najarian, "An endoscopic force-position sensor grasper with minimum sensors," *Can. J. Electr. Comput. Eng.*, vol. 28, nos. 3–4, pp. 155–161, Jul. 2003.

[19] S. Najarian, J. Dargahi, and A. A. Mehrizi, *Artificial Tactile Sensing in Biomedical Engineering*. New York, NY, USA: McGraw-Hill, 2009.

[20] S. Najarian, J. Dargahi, G. Darbemamieh, and S. H. Farkoush, *Mechatronics in Medicine a Biomedical Engineering Approach*. New York, NY, USA: McGraw-Hill, 2011.

[21] M. Tanimoto, F. Arai, T. Fukuda, H. Iwata, K. Itoigawa, Y. Gotoh, M. Hashimoto, and M. Negoro, "Micro force sensor for intravascular neurosurgery and *in vivo* experiment," in *Proc. IEEE. 11th Annu. Int. Workshop Micro Electro Mech. Syst. Invest. Micro Struct., Sensors, Actuat., Machines Syst. (MEMS)*, Nov. 2002, pp. 504–509.

[22] C.-H. King, M. Culjat, M. Franco, J. Bisley, G. Carman, E. Dutson, and W. Grundfest, "A multielement tactile feedback system for robot–assisted minimally invasive surgery," *IEEE Trans. Haptics*, vol. 2, no. 1, pp. 52–56, Jan. 2009.

[23] C.-H. King, M. Culjat, M. Franco, C. Lewis, E. Dutson, W. Grundfest, and J. Bisley, "Tactile feedback induces reduced grasping force in robot–assisted surgery," *IEEE Trans. Haptics*, vol. 2, no. 2, pp. 103–110, Apr. 2009.

[24] Y. Hu, R. B. Katragadda, H. Tu, Q. Zheng, Y. Li, and Y. Xu, "Bioinspired 3-D tactile sensor for minimally invasive surgery," *J. Microelectromech. Syst.*, vol. 19, no. 6, pp. 1400–1408, Dec. 2010.

[25] K. Zareinia, Y. Maddahi, L. S. Gan, A. Ghasemloonia, S. Lama, T. Sugiyama, F. W. Yang, and G. R. Sutherland, "A force–sensing bipolar forceps to quantify tool–tissue interaction forces in microsurgery," *IEEE/ASME Trans. Mechatronics*, vol. 21, no. 5, pp. 2365–2377, Oct. 2016.

[26] K. Weiss and H. Woern, "Tactile sensor system for an anthropomorphic robotic hand," in *Proc. IEEE Int. Conf. Manipulation Grasping (IMG)*, Kobe, Japan, vol. 1217, May 2004, Art. no. 895901.

[27] N. Bandari, J. Dargahi, and M. Packirisamy, "Validation of a variable bending radius sensing principle for optical-fiber tactile sensors," in *Proc. Photon. North (PN)*, May 2019, p. 1.

[28] S. Sokhanvar, M. Packirisamy, and J. Dargahi, "MEMS endoscopic tactile sensor: Toward *in-situ* and *in-vivo* tissue softness characterization," *IEEE Sensors J.*, vol. 9, no. 12, pp. 1679–1687, Dec. 2009.

[29] A. H. King, "The science and engineering of materials," *Mater. Sci. Eng., A*, vol. 212, no. 1, pp. 186–187, Jul. 1996.

[30] A. Eklund, A. Bergh, and O. A. Lindahl, "A catheter tactile sensor for measuring hardness of soft tissue: Measurement in a silicone model and in an *in vitro* human prostate model," *Med. Biol. Eng. Comput.*, vol. 37, no. 5, pp. 618–624, Sep. 1999.

[31] C.-H. Chuang, T.-H. Li, I.-C. Chou, and Y.-J. Teng, "Piezoelectric tactile sensor for submucosal tumor detection in endoscopy," *Sens. Actuators A, Phys.*, vol. 244, pp. 299–309, Jun. 2016.

[32] S. Sharma, R. Aguilera, J. Rao, and J. K. Gimzewski, "Piezoelectric needle sensor reveals mechanical heterogeneity in human thyroid tissue lesions," *Sci. Rep.*, vol. 9, no. 1, p. 9282, Dec. 2019.

[33] R. Smith-Bindman, P. Lebda, V. A. Feldstein, D. Sellami, R. B. Goldstein, N. Brasic, C. Jin, and J. Kornak, "Risk of thyroid cancer based on thyroid ultrasound imaging characteristics: Results of a population-based study," *JAMA Internal Med.*, vol. 173, no. 19, pp. 1788–1795, 2013.

[34] M. Eltaib and J. Hewit, "A tactile sensor for minimal access surgery applications," *IFAC Proc. Volumes*, vol. 33, no. 26, pp. 505–508, Sep. 2000.

[35] P. Peng, R. Rajamani, and A. Erdman, "Flexible tactile sensor for tissue elasticity measurements," *J. Microelectromech. Syst.*, vol. 18, no. 6, pp. 1226–1233, Dec. 2009.

[36] O. H. Paydar, C. R. Wottawa, R. E. Fan, E. P. Dutson, W. S. Grundfest, M. O. Culjat, and R. N. Candler, "Fabrication of a thin-film capacitive force sensor array for tactile feedback in robotic surgery," in *Proc. Annu. Int. Conf. IEEE Eng. Med. Biol. Soc.*, Aug. 2012, pp. 2355–2358.

[37] U. Kim, Y. B. Kim, J. So, D.-Y. Seok, and H. R. Choi, "Sensorized surgical forceps for robotic–assisted minimally invasive surgery," *IEEE Trans. Ind. Electron.*, vol. 65, no. 12, pp. 9604–9613, Dec. 2018.

[38] M. B. Hong and Y.-H. Jo, "Design of a Novel 4-DOF wrist–type surgical instrument with enhanced rigidity and dexterity," *IEEE/ASME Trans. Mechatronics*, vol. 19, no. 2, pp. 500–511, Apr. 2014.

[39] L. C. Clark, R. Wolf, D. Granger, and Z. Taylor, "Continuous recording of blood oxygen tensions by polarography," *J. Appl. Physiol.*, vol. 6, no. 3, pp. 189–193, Sep. 1953.

[40] S. Nemoto and T. Makimoto, "Analysis of splice loss in single-mode fibres using a Gaussian field approximation," *Opt. Quant. Electron.*, vol. 11, no. 5, pp. 447–457, Sep. 1979.

[41] O. Tohyama, M. Kohashi, K. Yamamoto, and H. Itoh, "A fiber-optic silicon pressure sensor for ultra-thin catheters," *Sens. Actuators A, Phys.*, vol. 54, nos. 1–3, pp. 622–625, Jun. 1996.

[42] M. L. Polanyi and R. M. Hehir, "New reflection oximeter," *Rev. Sci. Instrum.*, vol. 31, no. 4, pp. 401–403, Apr. 1960.
[43] P. L. Frommer, J. Ross, D. T. Mason, J. H. Gault, and E. Braunwald, "Clinical applications of an improved, rapidly responding fiberoptic catheter," *Amer. J. Cardiol.* , vol. 15, no. 5, pp. 672–679, May 1965.
[44] J. Heijmans, L. Cheng, and F. Wieringa, "Optical fiber sensors for medical applications—Practical engineering considerations," in *Proc. 4th Eur. Conf. Int. Fed. Med. Biol. Eng.* Berlin, Germany: Springer, 2009, pp. 2330–2334.
[45] I. Gannot, "Optical fibers and sensors for medical applications," *Proc. SPIE*, vol. 4253, pp. 933–936, Jun. 2001.
[46] J. Dargahi, M. Parameswaran, and S. Payandeh, "A micromachined piezoelectric tactile sensor for an endoscopic grasper-theory, fabrication and experiments," *J. Microelectromech. Syst.*, vol. 9, no. 3, pp. 329–335, Sep. 2000.
[47] N. Kattavenos, B. Lawrenson, T. Frank, M. Pridham, R. Keatch, and A. Cuschieri, "Force–sensitive tactile sensor for minimal access surgery," *Minimally Invasive Therapy Allied Technol.*, vol. 13, no. 1, pp. 42–46, Jan. 2004.
[48] M. Ottermo, O. Stavdahl, and T. Johansen, "Palpation instrument for augmented minimally invasive surgery," in *Proc. IEEE/RSJ Int. Conf. Intell. Robots Syst. (IROS)*, Apr. 2005, pp. 3960–3964.
[49] M. A. Qasaimeh, S. Sokhanvar, J. Dargahi, and M. Kahrizi, "A micro-tactile sensor for *in situ* tissue characterization in minimally invasive surgery," *Biomed. Microdevices*, vol. 10, no. 6, pp. 823–837, Dec. 2008.
[50] A. L. Trejos, R. V. Patel, M. D. Naish, A. C. Lyle, and C. M. Schlachta, "A sensorized instrument for skills assessment and training in minimally invasive surgery," *J. Med. Devices*, vol. 3, no. 4, Dec. 2009, Art. no. 041002.
[51] A. T. Golpaygani, S. Najarian, and M. Movahedi, "Tactile sensor for robotic applications," in *World Congress on Medical Physics and Biomedical Engineering*, Munich, Germany: Springer, Sep. 2009, pp. 2299–2302.
[52] V. Jalkanen, "Hand-held resonance sensor for tissue stiffness measurements—A theoretical and experimental analysis," *Meas. Sci. Technol.*, vol. 21, no. 5, 2010, Art. no. 055801.
[53] M. Kalantari, M. Ramezanifard, R. Ahmadi, J. Dargahi, and J. Kövecses, "A piezoresistive tactile sensor for tissue characterization during catheter-based cardiac surgery," *Int. J. Med. Robot. Comput. Assist. Surg.*, vol. 7, no. 4, pp. 431–440, Dec. 2011.
[54] P. Baki, G. Szekely, and G. Kosa, "Miniature tri-axial force sensor for feedback in minimally invasive surgery," in *Proc. 4th IEEE RAS EMBS Int. Conf. Biomed. Robot. Biomechtron. (BioRob)*, Jun. 2012, pp. 805–810.
[55] A. Talasaz and R. V. Patel, "Integration of force reflection with tactile sensing for minimally invasive robotics–assisted tumor localization," *IEEE Trans. Haptics*, vol. 6, no. 2, pp. 217–228, Apr. 2013.
[56] J.-H. Hwang, J. Ho Kwon, T.-K. Kim, and D. Hong, "Design of simple structured tactile sensor for the minimally invasive robotic palpation," in *Proc. IEEE/ASME Int. Conf. Adv. Intell. Mechatronics*, Jul. 2013, pp. 1296–1299.
[57] J. Lee, W. Choi, Y. Yoo, K. Hwang, S.-M. Lee, S. Kang, J. Kim, and J. Lee, "A micro–fabricated force sensor using an all thin film piezoelectric active sensor," *Sensors*, vol. 14, no. 12, pp. 22199–22207, Nov. 2014.
[58] K. Li, B. Pan, J. Zhan, W. Gao, Y. Fu, and S. Wang, "Design and performance evaluation of a 3-axis force sensor for MIS palpation," *Sensor Rev.*, vol. 35, no. 2, pp. 219–228, Mar. 2015.
[59] U. Kim, D.-H. Lee, W. J. Yoon, B. Hannaford, and H. R. Choi, "Force sensor integrated surgical forceps for minimally invasive robotic surgery," *IEEE Trans. Robot.*, vol. 31, no. 5, pp. 1214–1224, Oct. 2015.
[60] M. Hessinger, T. Pilic, R. Werthschutzky, and P. P. Pott, "Miniaturized force/torque sensor for *in vivo* measurements of tissue characteristics," in *Proc. 38th Annu. Int. Conf. IEEE Eng. Med. Biol. Soc. (EMBC)*, Aug. 2016, pp. 2022–2025.
[61] L. Zhang, F. Ju, Y. Cao, Y. Wang, and B. Chen, "A tactile sensor for measuring hardness of soft tissue with applications to minimally invasive surgery," *Sens. Actuators A, Phys.*, vol. 266, pp. 197–204, Oct. 2017.
[62] U. Kim, Y. B. Kim, D.-Y. Seok, J. So, and H. R. Choi, "A surgical palpation probe with 6-axis force/torque sensing capability for minimally invasive surgery," *IEEE Trans. Ind. Electron.*, vol. 65, no. 3, pp. 2755–2765, Mar. 2018.
[63] J. Radó, C. Dücső, P. Földesy, G. Szebényi, Z. Nawrat, K. Rohr, and P. Fürjes, "3D force sensors for laparoscopic surgery tool," *Microsyst. Technol.*, vol. 24, no. 1, pp. 519–525, Jan. 2018.
[64] F. Ju, Y. Wang, Z. Zhang, Y. Wang, Y. Yun, H. Guo, and B. Chen, "A miniature piezoelectric spiral tactile sensor for tissue hardness palpation with catheter robot in minimally invasive surgery," *Smart Mater. Struct.*, vol. 28, no. 2, Feb. 2019, Art. no. 025033.
[65] U. Kim, Y. B. Kim, D.-Y. Seok, and H. R. Choi, "S–surge: A portable surgical robot based on a novel mechanism with force–sensing capability for robotic surgery," in *Handbook Robotic Image-Guided Surgery*. Amsterdam, The Netherlands: Elsevier, 2020, pp. 265–283.
[66] R. C. Gauthier and C. Ross, "Theoretical and experimental considerations for a single-mode fiber-optic bend-type sensor," *Appl. Opt.*, vol. 36, no. 25, p. 6264, Sep. 1997.
[67] N. Lagakos, J. H. Cole, and J. A. Bucaro, "Microbend fiber-optic sensor," *Appl. Opt.*, vol. 26, no. 11, p. 2171, Jun. 1987.
[68] J. Faria, "A theoretical analysis of the bifurcated fiber bundle displacement sensor," *IEEE Trans. Instrum. Meas.*, vol. 47, no. 3, pp. 742–747, Jun. 1998.
[69] P. Polygerinos, L. D. Seneviratne, and K. Althoefer, "Modeling of light intensity–modulated fiber–optic displacement sensors," *IEEE Trans. Instrum. Meas.*, vol. 60, no. 4, pp. 1408–1415, Apr. 2011.
[70] R. Ahmadi, M. Packirisamy, J. Dargahi, and R. Cecere, "Discretely loaded beam–type optical fiber tactile sensor for tissue manipulation and palpation in minimally invasive robotic surgery," *IEEE Sensors J.*, vol. 12, no. 1, pp. 22–32, Jan. 2012.
[71] N. M. Bandari, A. Hooshair, M. Packirisamy, and J. Dargahi, "Optical fiber array sensor for lateral and circumferential force measurement suitable for minimally invasive surgery: Design, modeling and analysis," in *Proc. Specialty Opt. Fibers. Opt. Soc. Amer.*, 2016, pp. 1–2, Paper JTu4A–44.
[72] R. Ahmadi, "Innovative optical microsystem for static and dynamic tissue diagnosis in minimally invasive surgical operations," *J. Biomed. Opt*, vol. 17, no. 8, Aug. 2012, Art. no. 081416.
[73] B. Gersak and Z. Sutlic, "Aortic and mitral valve surgery on the beating heart is lowering cardiopulmonary bypass and aortic cross clamp time," *Heart Surg. Forum*, vol. 5, no. 2, pp. 182–186, 2002.
[74] M. C. Yip, S. G. Yuen, and R. D. Howe, "A robust uniaxial force sensor for minimally invasive surgery," *IEEE Trans. Biomed. Eng.*, vol. 57, no. 5, pp. 1008–1011, May 2010.
[75] Y. Noh, H. Liu, S. Sareh, D. S. Chathuranga, H. Wurdemann, K. Rhode, and K. Althoefer, "Image–based optical miniaturized three–axis force sensor for cardiac catheterization," *IEEE Sensors J.*, vol. 16, no. 22, pp. 7924–7932, Nov. 2016.
[76] M. Atoui, S. Gunda, D. Lakkireddy, and S. Mahapatra, "Radiofrequency ablation to prevent sudden cardiac death," *Methodist DeBakey Cardiovascular J.*, vol. 11, no. 2, pp. 121–128, Apr. 2015.
[77] K. O. Hill, Y. Fujii, D. C. Johnson, and B. S. Kawasaki, "Photosensitivity in optical fiber waveguides: Application to reflection filter fabrication," *Appl. Phys. Lett.*, vol. 32, no. 10, pp. 647–649, May 1978.
[78] G. Meltz, W. W. Morey, and W. H. Glenn, "Formation of Bragg gratings in optical fibers by a transverse holographic method," *Opt. Lett.*, vol. 14, no. 15, p. 823, Aug. 1989.
[79] Y.-L. Park, S. Elayaperumal, B. Daniel, S. C. Ryu, M. Shin, J. Savall, R. J. Black, B. Moslehi, and M. R. Cutkosky, "Real-time estimation of 3-d needle shape and deflection for mri-guided interventions," *IEEE/ASME Trans. Mechatronics*, vol. 15, no. 6, pp. 906–915, Dec. 2010.
[80] T. Lehmann, M. Tavakoli, N. Usmani, and R. Sloboda, "Force-sensor-based estimation of needle tip deflection in Brachytherapy," *J. Sensors*, vol. 2013, Apr. 2013, Art. no. 263153.
[81] T. Lehmann, R. Sloboda, N. Usmani, and M. Tavakoli, "Model–based needle steering in soft tissue via lateral needle actuation," *IEEE Robot. Autom. Lett.*, vol. 3, no. 4, pp. 3930–3936, Oct. 2018.
[82] P. S. Zarrin, A. Escoto, R. Xu, R. V. Patel, M. D. Naish, and A. L. Trejos, "Development of a 2-DOF sensorized surgical grasper for grasping and axial force measurements," *IEEE Sensors J.*, vol. 18, no. 7, pp. 2816–2826, Apr. 2018.
[83] P. S. Zarrin, A. Escoto, R. Xu, R. V. Patel, M. D. Naish, and A. L. Trejos, "Development of an optical fiber-based sensor for grasping and axial force sensing," in *Proc. IEEE Int. Conf. Robot. Autom. (ICRA)*, May 2017, pp. 939–944.
[84] F. Taffoni, D. Formica, P. Saccomandi, G. Pino, and E. Schena, "Optical fiber–based mr–compatible sensors for medical applications: An overview," *Sensors*, vol. 13, no. 10, pp. 14105–14120, Oct. 2013.
[85] W. Shang, H. Su, G. Li, C. Furlong, and G. S. Fischer, "A Fabry–Pérot interferometry based MRI-compatible miniature uniaxial force sensor for percutaneous needle placement," in *Proc. IEEE SENSORS*, Nov. 2013, pp. 1–4.

[86] H. Su, M. Zervas, G. A. Cole, C. Furlong, and G. S. Fischer, "Real-time MRI-guided needle placement robot with integrated fiber optic force sensing," in *Proc. IEEE Int. Conf. Robot. Autom.*, May 2011, pp. 1583–1588.
[87] M. Islam, M. Ali, M.-H. Lai, K.-S. Lim, and H. Ahmad, "Chronology of Fabry–Pérot interferometer fiber–optic sensors and their applications: A review," *Sensors*, vol. 14, no. 4, pp. 7451–7488, Apr. 2014.
[88] B. H. Lee, Y. H. Kim, K. S. Park, J. B. Eom, M. J. Kim, B. S. Rho, and H. Y. Choi, "Interferometric fiber optic sensors," *Sensors*, vol. 12, no. 3, pp. 2467–2486, 2012.
[89] T. K. Gangopadhyay, "Prospects for Fibre Bragg gratings and Fabry–Pérot interferometers in fibre-optic vibration sensing," *Sens. Actuators A, Phys.*, vol. 113, no. 1, pp. 20–38, Jun. 2004.
[90] H. Su, D. C. Cardona, W. Shang, A. Camilo, G. A. Cole, D. C. Rucker, R. J. Webster, and G. S. Fischer, "A MRI-guided concentric tube continuum robot with piezoelectric actuation: A feasibility study," in *Proc. IEEE Int. Conf. Robot. Autom.*, May 2012, pp. 1939–1945.
[91] Z. Mo and W. Xu, "Temperature–compensated optical fiber force sensing at the tip of a surgical needle," *IEEE Sensors J.*, vol. 16, no. 24, pp. 8936–8943, Dec. 2016.
[92] Z. Ran, Y. Rao, J. Zhang, Z. Liu, and B. Xu, "A miniature fiber-optic refractive-index sensor based on laser-machined Fabry–Pérot interferometer tip," *J. Lightw. Technol.*, vol. 27, no. 23, pp. 5426–5429, Dec. 1, 2009.
[93] Y.-J. Rao, M. Deng, D.-W. Duan, X.-C. Yang, T. Zhu, and G.-H. Cheng, "Micro Fabry–Pérot interferometers in silica fibers machined by femtosecond laser," *Opt. Express*, vol. 15, no. 21, pp. 14123–14128, 2007.
[94] V. Machavaram, R. Badcock, and G. Fernando, "Fabrication of intrinsic fibre Fabry–Pérot sensors in silica fibres using hydrofluoric acid etching," *Sens. Actuators A, Phys.*, vol. 138, no. 1, pp. 248–260, Jul. 2007.
[95] D. J. Webb, M. W. Hathaway, D. A. Jackson, S. Jones, L. Zhang, and I. Bennion, "First *in-vivo* trials of a fiber Bragg grating based temperature profiling system," *J. Biomed. Opt.*, vol. 5, no. 1, p. 45, 2000.
[96] M. Tada, S. Sasaki, and T. Ogasawara, "Development of an optical 2-axis force sensor usable in MRI environments," in *Proc. IEEE Sensors*, vol. 2, Jun. 2003, pp. 984–989.
[97] D. Chapuis, R. Gasseri, L. Sache, E. Burdet, and H. Bleuler, "Design of a simple MRI/fMRI compatible force/torque sensor," in *Proc. IEEE/RSJ Int. Conf. Intell. Robots Syst. (IROS)*, vol. 3, Sep. 2005, pp. 2593–2599.
[98] H. Su and G. S. Fischer, "A 3-axis optical force/torque sensor for prostate needle placement in Magnetic resonance imaging environments," in *Proc. IEEE Int. Conf. Technol. Practical Robot Appl.*, Nov. 2009, pp. 5–9.
[99] M. S. Müller, L. Hoffmann, T. C. Buck, and A. W. Koch, "Fiber Bragg grating–based force–torque sensor with six degrees of freedom," *Int. J. Optomechtron.*, vol. 3, no. 3, pp. 201–214, Sep. 2009.
[100] P. Polygerinos, T. Schaeffter, L. Seneviratne, and K. Althoefer, "A fibre-optic catheter-tip force sensor with MRI compatibility: A feasibility study," in *Proc. Annu. Int. Conf. IEEE Eng. Med. Biol. Soc.*, Sep. 2009, pp. 1054–1501.
[101] S. B. Kesner and R. D. Howe, "Design principles for rapid prototyping forces sensors using 3-D printing," *IEEE/ASME Trans. Mechatronics*, vol. 16, no. 5, pp. 866–870, Oct. 2011.
[102] X. Liu, I. I. Iordachita, X. He, R. H. Taylor, and J. U. Kang, "Miniature fiber-optic force sensor based on low-coherence Fabry-Pérot interferometry for vitreoretinal microsurgery," *Biomed. Opt. Express*, vol. 3, no. 5, pp. 1062–1076, 2012.
[103] P. Polygerinos, L. D. Seneviratne, R. Razavi, T. Schaeffter, and K. Althoefer, "Triaxial Catheter–Tip Force Sensor for MRI–Guided Cardiac Procedures," *IEEE/ASME Trans. Mechatronics*, vol. 18, no. 1, pp. 386–396, Feb. 2013.
[104] S. Elayaperumal, J. H. Bae, B. L. Daniel, and M. R. Cutkosky, "Detection of membrane puncture with haptic feedback using a tip-force sensing needle," in *Proc. IEEE/RSJ Int. Conf. Intell. Robots Syst.*, Sep. 2014, pp. 3975–3981.
[105] R. Ahmadi, S. Arbatani, M. Packirisamy, and J. Dargahi, "Micro-optical force distribution sensing suitable for lump/artery detection," *Biomed Microdevices*, vol. 17, no. 1, p. 10, Feb. 2015.
[106] Z. Mo, W. Xu, and N. Broderick, "A Fabry–Pérot optical fiber force sensor based on intensity modulation for needle tip force sensing," in *Proc. 6th Int. Conf. Autom., Robot. Appl. (ICARA)*, Feb. 2015, pp. 376–380.
[107] Y. Qiu, Y. Wang, Y. Xu, N. Chandra, J. Haorah, B. Hubbi, B. J. Pfister, and X. Liu, "Quantitative optical coherence elastography based on fiber-optic probe for *in situ* measurement of tissue mechanical properties," *Biomed. Opt. Express*, vol. 7, no. 2, p. 688, Feb. 2016.
[108] T. Li, C. Shi, and H. Ren, "A high–sensitivity tactile sensor array based on fiber Bragg grating sensing for tissue palpation in minimally invasive surgery," *IEEE/ASME Trans. Mechatronics*, vol. 23, no. 5, pp. 2306–2315, Oct. 2018.
[109] I. B. Wanninayake, "Miniaturised optical fibre based palpations instrument for minimally invasive surgery," *J. Phys., Conf. Ser.*, vol. 1151, Jan. 2019, Art. no. 012014.
[110] D. Tosi, E. G. Macchi, G. Braschi, A. Cigada, M. Gallati, S. Rossi, S. Poeggel, G. Leen, and E. Lewis, "Fiber-optic combined FPI/FBG sensors for monitoring of radiofrequency thermal ablation of liver tumors: Ex vivo experiments," *Appl. Opt.*, vol. 53, no. 10, p. 2136, Apr. 2014.
[111] N. M. Bandari, R. Ahmadi, A. Hooshiar, J. Dargahi, and M. Packirisamy, "Hybrid piezoresistive-optical tactile sensor for simultaneous measurement of tissue stiffness and detection of tissue discontinuity in robot-assisted minimally invasive surgery," *J. Biomed. Opt*, vol. 22, no. 7, Jul. 2017, Art. no. 077002.
[112] T. Köhler, S. Haase, S. Bauer, J. Wasza, T. Kilgus, L. Maier-Hein, H. Feußner, and J. Hornegger, "Tof meets RGB: Novel multi-sensor super-resolution for hybrid 3-D endoscopy," in *Proc. Int. Conf. Med. Image Comput. Comput.-Assist. Intervent*. Berlin, Germany: Springer, 2013, pp. 139–146.
[113] M. Fajkus, J. Nedoma, R. Martinek, V. Vasinek, H. Nazeran, and P. Siska, "A non-invasive multichannel hybrid fiber-optic sensor system for vital sign monitoring," *Sensors*, vol. 17, no. 12, p. 111, Jan. 2017.
[114] K. Konishi, M. Nakamoto, Y. Kakeji, K. Tanoue, H. Kawanaka, S. Yamaguchi, S. Ieiri, Y. Sato, Y. Maehara, S. Tamura, and M. Hashizume, "A real-time navigation system for laparoscopic surgery based on three-dimensional ultrasound using magneto-optic hybrid tracking configuration," *Int. J. CARS*, vol. 2, no. 1, pp. 1–10, Jun. 2007.
[115] U. Bhattarai and A. T. Alouani, "Hybrid navigation information system for minimally invasive surgery: Offline sensors registration," in *Proc. Sci. Inf. Conf.* Cham, Switzerland: Springer, 2019, pp. 205–219.
[116] M. S. D. Zan, M. M. Elgaud, and A. A. A. Bakar, "Coding the optical pulse in TDM-FBG sensors with hybrid simplex-and golay codes for SNR improvement," in *Proc. 24th Opto Electron. Commun. Conf. (OECC) Int. Conf. Photon. Switching Comput. (PSC)*, Jul. 2019, pp. 1–3.
[117] B. D. Hoffman, D. Q. Larkin, G. M. Prisco, G. G. Zhang, and R. Kumar, "Methods and system for performing 3-D tool tracking by fusion of sensor and/or camera derived data during minimally invasive robotic surgery," U.S. Patent 16 396 125, Aug. 15, 2019.
[118] T. G. Thuruthel, B. Shih, C. Laschi, and M. T. Tolley, "Soft robot perception using embedded soft sensors and recurrent neural networks," *Sci. Robot.*, vol. 4, no. 26, Jan. 2019, Art. no. eaav1488.
[119] Z. Guo, C. Xing, C. Ke, K. Yang, and D. Liu, "3D shape sensing utilizing SBS in multi-core fiber," in *Proc. Opt. Fiber Commun. Conf. (OFC)*, Mar. 2019, pp. 1–3.
[120] M. Jolaei, A. Hooshiar, and J. Dargahi, "Displacement-based model for estimation of contact force between RFA catheter and atrial tissue with ex-vivo validation," in *Proc. IEEE Int. Symp. Robotic Sensors Environ. (ROSE)*, Jun. 2019, pp. 1–7.
[121] R. Wang, S. Wang, E. Xiao, K. Jindal, W. Yuan, and C. Feng, "Real-time soft body 3D proprioception via deep vision-based sensing," 2019, *arXiv:1904.03820*. [Online]. Available: https://arxiv.org/abs/1904.03820

NAGHMEH BANDARI received the bachelor's and master's degrees in biomedical engineering from the Amirkabir University of Technology, Tehran, Iran. She is currently pursuing the Ph.D. degree in mechanical engineering with Optical-Bio-MEMS and Robotic Surgery Labs, Concordia University, Montreal, QC, Canada. She later served as a certified medical device technical supervisor for six years in Iran. Her research interests include the development of optical tactile sensors and micro-optical mechanical systems for robot-assisted surgery applications. She is also a Fellow of surgical innovation of the NSERC CREATE Program for Innovation-at-the-Cutting-Edge (ICE) with McGill University. She received the FRQNT B2X Doctoral Scholarship for her interdisciplinary doctoral research and FRQNT CCTT Award for her collaboration with Optech CCTT, Montreal.

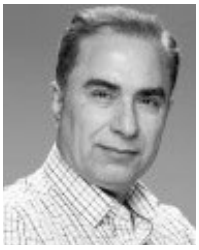

JAVAD DARGAHI received the Ph.D. degree in robotic tactile sensing from Glasgow Caledonian University, Glasgow, U.K., in 1993. In 2001, he joined the Department of Mechanical and Industrial Engineering, Concordia University, as an Assistant Professor, where he was promoted to a Full Professor, in 2011. He has published more than 150 journals and conference papers. He holds several patents and three books. He is the coauthor of a book *Artificial Tactile Sensing in Biomedical Engineering* (McGraw-Hill). He holds a patent titled System for Sensing and Displaying Force and Softness. His research interests include the design and fabrication of haptic sensors and feedback systems for minimally invasive surgery and robotics, and micromachined sensors and actuators.

MUTHUKUMARAN PACKIRISAMY received the B.E. degree in mechanical engineering from the University of Madras, Chennai, India, the M.S. degree in mechanical engineering from the IIT Madras, India, and the Ph.D. degree in mechanical engineering from Concordia University, Montreal, Canada. He is a Professor and the Concordia Research Chair of the Department of Mechanical Engineering, Concordia University. As an expert in the areas of micro-nano-bio integration, optical bio microsystems, *in situ* and *ex situ* nano integration of lab on chip and microsensors, he develops and studies nano integrated microsystems for various applications. As the Director of the Micro-Nano-Bio Integration Center and Optical Bio Microsystems Laboratory, he developed this lab focusing on lab on chip, bio-microsystems, and micro-nano integration. He was a recipient of the Member Royal Society of Canada College, the I. W. Smith Award from Canadian Society for Mechanical Engineering, the Concordia University Research Fellowship, the Petro Canada Young Innovator Award, and the ENCS Young Research Achievement Award. He was a Fellow of the National Academy of Inventors, USA, the Indian National Academy of Engineering, the Engineering Institute of Canada, Canadian Academy of Engineering, the American Society of Mechanical Engineers, the Institution of Engineers India, and the Canadian Society for Mechanical Engineering. As an author of around 440 articles published in journals and conference proceedings and 42 invited talks, he has 30 inventions in the micro and nano systems.